The Design of Skin Friction Gages for Measurements in High-Speed, Short-Duration Flows

by

John F. Busic

Thesis submitted to the faculty of the

Virginia Polytechnic Institute and State University

in partial fulfillment of the requirements for the degree of

Master of Science

in

Mechanical Engineering

APPROVED:

Thomas E. Diller, Chairman

Alfred L. Wicks

Joseph A. Schetz

July, 1992

Blacksburg, Virginia

The Design of Skin Friction Gages for Measurements in High-Speed, Short-Duration Flows

by

John F. Busic

Committee Chairman: Thomas E. Diller

Mechanical Engineering

ABSTRACT

The design of skin friction gages has been explored analytically and experimentally for measuring skin friction in high-speed, short-duration flow. Several gage designs were considered. One promising gage design used a floating element, while another was microfabricated using sputtering techniques. All of the gages were physically modeled to determine the output caused by Mach 2 unheated flow. Frequency response analysis was also performed on the floating element and sputtered design to determine their ability to make measurements in the millisecond time range. Temperature and normal pressure effects were a source of measurement error, and techniques were developed for minimizing the error due these effects. Tests were made in Mach 2 flow and the results of these tests are discussed. Recommendations are provided as to how the gages can be improved for further testing.

ABSTRACT

Acknowledgements

I would like to thank Dr. Thomas Diller for being my advisor throughout graduate school. His patience and guidance during this research is greatly appreciated. Gratitude is also expressed toward the other members of my committee as well as my colleagues.

I also would like to thank my wife for her support and excellent typing skills without which I never would have made it. Thanks also are expressed to my parents (The best teachers I ever had!) for encouraging me throughout my educational experience.

Contents

List of Figures

List of Tables

Nomenclature

A_s	Surface area of sensing head
A,B	Hot-wire power / shear stress relationship constants
C_f	Skin friction coefficient
CF	Correction factor for Wheatstone quarter bridge
cm	Centimeter
d	Preston tube inner diameter
D	Preston tube outer diameter
e	Electrical power or strain
E_{AB}	Voltage potential across leg AB
E_{AD}	Voltage potential across leg AD
E_{out}	Voltage output from Wheatstone bridge
E_{in}	Voltage input from Wheatstone bridge
ΔE_{out}	Change in voltage output from Wheatstone bridge
g	gravitational acceleration
GF	Gage factor of strain gage
h	Channel height for Stanton tube, height of viscous fluid in viscometer
m	mass of sensing head for T-top gage
Pa	Pascal
P	Static pressure
P_T	Total pressure
ΔP	$P_T - P$
r	Radial distance of gage from center of rotation
ΔR	Change in resistance
R	Resistance
R_1	Resistance in one leg of the Wheatstone bridge
R_2	Resistance in one leg of the Wheatstone bridge
R_3	Resistance in one leg of the Wheatstone bridge
R_4	Resistance in one leg of the Wheatstone bridge
S	Magnitude of velocity gradient at the wall
t	Time
T_f	Temperature of heated element
T_∞	Free stream temperature of the fluid
ΔT	$T_f - T_\infty$
u	Fluid velocity component in the x direction
U	Streamwise velocity of the fluid
V	Volts
W	Width of mass transfer element
y	Direction normal to test plate

α	Thermal diffusivity
δ	Thickness of insulating ring
δ_c	Thickness of concentration boundary layer
ρ	Density
τ	Shear stress
τ_w	Wall shear stress
μ	Viscosity
ν	Kinematic viscosity
ω	Angular velocity

Chapter 1

INTRODUCTION

1.1 RATIONALE FOR THE RESEARCH

The measurement of skin friction is an important task in analyzing a flow field. Skin friction measurement is also important because of the need to determine aerodynamic drag of aircraft, such as the National Aerospace Plane. In order for aircraft to reach hypersonic speeds, sufficient propulsion is needed to overcome the aerodynamic drag associated with the aircraft. The **S**upersonic **C**ombustion **RAMJET** (SCRAM-jet) engine, because of its impulse efficiency, simplicity, and relatively low structural loads shows promise in providing the propulsion necessary to reach these speeds.

The measurement of skin friction is desirable for propulsion research. Of considerable concern for the design of the SCRAM-jet engine is the level of internal skin friction caused by the combustion gases as they pass through the combustor. The amount of skin friction in relation to the cross-sectional area of the combustor has a controlling effect on the thrust produced by the SCRAMJET engine. The higher the

level of skin friction produced in the combustor, the lower the thrust available for propulsion of the aircraft.

Skin friction can be measured by either direct or indirect techniques. A direct measurement is preferred over an indirect measurement which has to be inferred from assumed or known properties of the flow. A review of some these direct and indirect methods of skin friction measurements is provided in the next chapter. In order to make skin friction measurements in a SCRAM-jet environment, direct measuring methods are needed. Indirect methods produce error because the basis for the various techniques are not well founded for 3-D, supersonic, combusting flows [1].

Different gage designs for measuring skin friction in high-speed, short-duration flows have been developed and evaluated. One gage uses a floating element design, while another is built using microfabrication techniques. Both gages are tested in Mach 2 unheated flow, to study their performance. The results are given as well as recommendations for gage improvement.

1.2 THESIS OVERVIEW

Chapter 1 gives a brief introduction which presents the rationale behind the need for accurate skin friction measurements. Chapter 2 includes the literature review section. This section reviews some of the traditional methods of skin friction measurement, such as Preston and Stanton tubes, thermal methods, and direct methods.

Chapter 3 deals with the testing apparatus. In this chapter such topics as data acquisition, skin friction gage calibration, and description of testing facilities are presented. Chapter 4 is the gage design process chapter. This chapter traces the development of the different gage designs, and gives the rationale behind each. As the chapter name suggests, this chapter begins with the original skin friction gage design and carries the reader through the research process and ends with improved skin friction gage designs. Chapter 5 finishes with the conclusions and recommendations for further improvement of the skin friction gages.

Chapter 2

LITERATURE REVIEW

Fluid flow over any surface exerts both static pressure and skin friction. Static pressure can be measured easily with static pressure taps and manometers or other pressure transducers. The measurement of the skin friction is not as easy, but the information obtained can be very rewarding because it is useful in analyzing the flow field. The measurement of skin friction can be accomplished by either direct or indirect methods.

2.1 INDIRECT METHODS

Indirect methods are so named because they measure some other quantity near the wall, and the skin friction is then determined based on assumed properties of the flow. Most of these indirect methods infer skin friction by the use of a Reynolds analogy, or some other assumed boundary layer approximations. The indirect methods used to measure skin friction consist of the Stanton tube, the Preston tube, the

sublayer fence, the electrochemical technique, and the thermal method. All these methods are covered in detail in chapter eleven of Fluid Mechanics Measurements [2].

2.1.1 STANTON TUBE

A Stanton tube can be made by placing a razor blade over a static pressure hole as shown in figure 2.1. The pressure developed in the enclosure of the razor blade is measured, and then calibrated for skin friction. The Stanton tube is generally placed on the wall, in the linear region of the velocity profile. Because the velocity profile is linear in this region, the skin friction is directly proportional to the velocity gradient as shown in equation 2.1.

$$\tau_w = \mu \left(\frac{\partial u}{\partial y} \right)_{y=0} \qquad [2.1]$$

The attractive features of this Stanton tube design are its small size, and its ease of implementation. East [3] performed a calibration of a Stanton tube in turbulent flow over a flat plate. East used the design shown in Figure 2.1, which had the unique feature of a magnet to hold the razor blade in place. The magnet avoided the use of glue and the unknown thickness that glue produces when used to hold down a

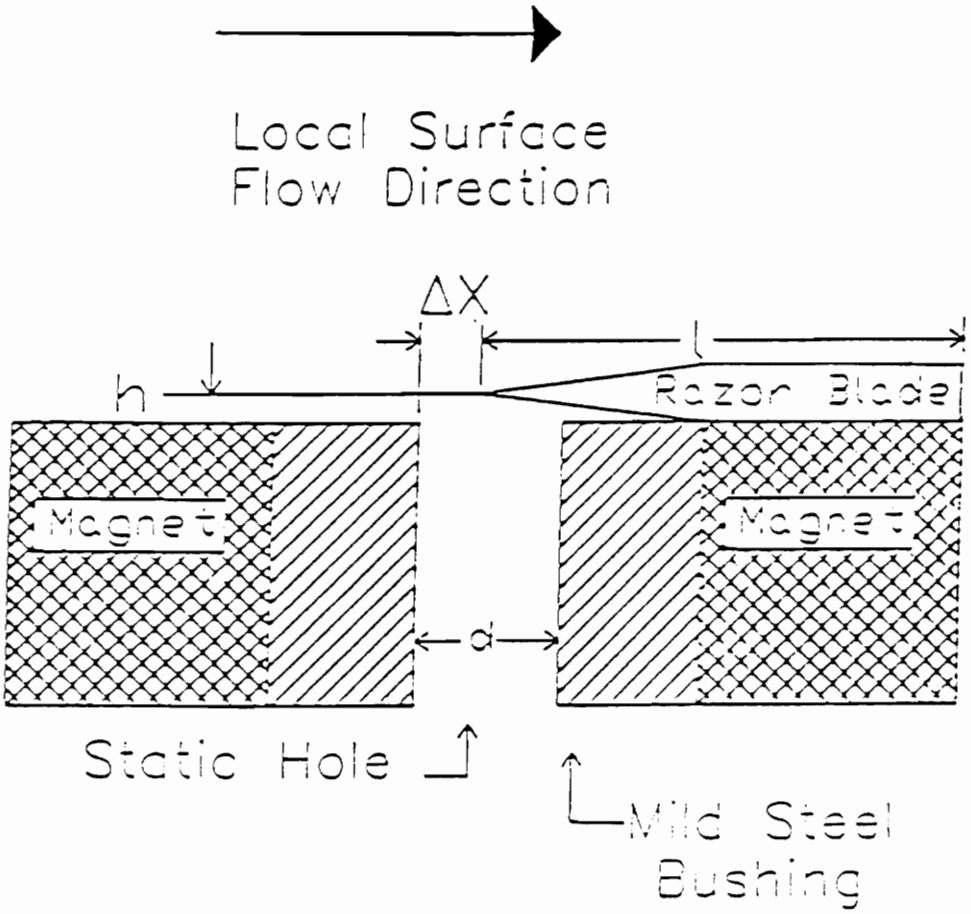

Figure 2.1 Design of Stanton gage as given by East

razor blade. East calibrated his Stanton Gage against a Preston tube and came up with the following calibration:

$$y^* = -0.23 + 0.618x^* + 0.0165(x^*)^2$$

where $2 < x^* < 6$

$$x^* = \log_{10}\left(\frac{\Delta P h^2 \rho}{\mu^2}\right) \qquad [2.2]$$

and

$$Y^* = \log_{10}\left(\frac{\overline{\tau_w} h^2 \rho}{\mu^2}\right) \qquad [2.3]$$

2.1.2 PRESTON TUBE

The Preston tube has long been used to infer skin friction in fluid flows because of its relative ease of use when compared with other indirect skin friction measurements. Preston used the Preston tube design shown in figure 2.2 to measure skin friction in turbulent flow. Preston [4] determined that a total pressure measurement made at a known distance from the wall could be used to infer the wall skin friction from the relationship given in equation [2.4].

$$\frac{\Delta P d^2}{\rho \nu^2} = f\left(\frac{\tau_w D^2}{\rho \nu^2}\right) \qquad [2.4]$$

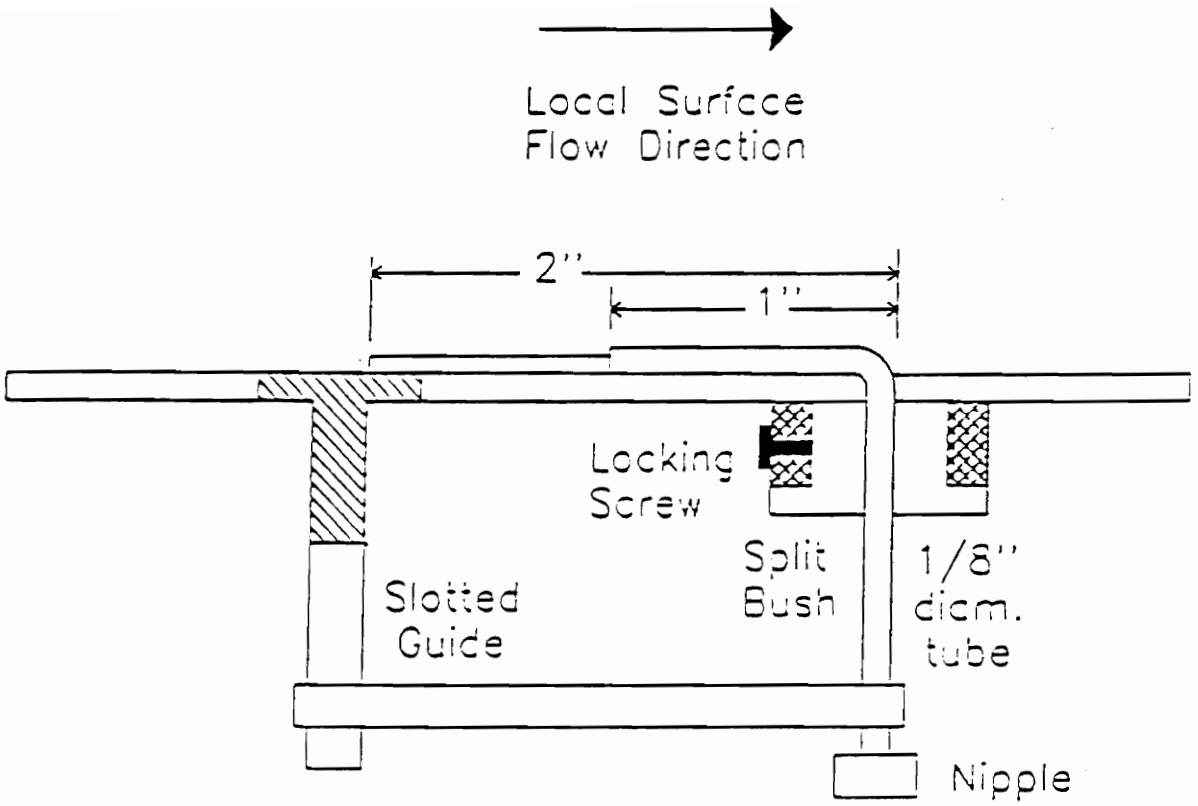

Figure 2.2 Schematic of Preston Tube [4]

Where ΔP is the total pressure minus the local static pressure, d is the inside tube diameter, and D is the outside tube diameter.

Most Preston tubes use an inside to outside diameter ratio of 0.6, but it has been shown by Patel [5] that the output is not too sensitive to this parameter provided that the ratio is greater than 0.2. Several different calibrations have been developed for Preston tube measurements. The Preston tube calibration presented here is considered to be one of the best [6]

Patel Preston tube calibration equations [5]

$$y^* = 0.5x^* + 0.037 \qquad x^* < 2.90$$

$$y^* = 0.8287 - 0.1381x^* + 0.1437x^{*2} - 0.006x^{*3} \qquad 2.9 \leq x^* < 5.6$$

$$x^* = y^* + 2\log_{10}(1.95y^* + 4.10) \qquad 5.6 < x^* < 7.6$$

where

$$x^* = \log_{10}\left(\frac{\Delta P D^2}{4\rho\nu^2}\right) \qquad [2.5]$$

and

$$y^* = \log_{10}\left(\frac{\tau_w D^2}{4\rho\nu^2}\right) \qquad [2.6]$$

Some limitations associated with the usage of the Preston tube is that the flow field's velocity profile needs to be two-dimensional and well defined. Also if the tube is small enough to be located totally within the logarithmic portion of the boundary layer, the Preston tube pressure measurement will be a function of the law of the wall.

When comparing the Stanton tube and the Preston tube, it appears that they are very similar. While it is true that some similarities exist, there are some important differences between the two. The Preston tube is considered to be a global device which measures Bernoulli type pressures, due to the deceleration of the fluid in front of the tube. The Stanton tube is a local device which enables it to respond more quickly to skin friction fluctuations. Also the Stanton tube is characterized by numerous physical parameters such as the overall height and width, and the opening height and

width. The many physical parameters associated with the Stanton tube complicates its operation and makes the calculations of skin friction more difficult than the Preston tube [2].

2.1.3 SUBLAYER FENCE

The sublayer fence is exactly what this name suggests. It consists of a small fence that is smaller than the viscous sublayer of the flow. Since the sublayer fence is smaller than the viscous sublayer, the law of the wall holds for the flow in this region. When there is flow over the fence, there exists a recirculation zone in front of and behind the fence creating a static pressure difference. Two static pressure taps are located on either side of the sublayer fence. The difference between the static pressure on either side of the fence can be calibrated against skin friction. Head and Rechenberg [7] did experiments calibrating a sublayer fence with a Preston tube in turbulent flow. The sublayer fence has an advantage over the Preston tube and Stanton tube in that it can measure both forward and reversed flow.

2.1.4 THERMAL METHOD

Most thermal methods use a heated film that is placed level with the wall where the skin friction is to be measured. A hot wire anemometer can be used to keep the heated film at a constant temperature. The corresponding electrical power, e, needed to maintain the temperature can be related to skin friction via the equation given by Fage and Falkner [8]:

$$\frac{e}{\Delta T} = A + B(\rho\tau)_w^{\frac{1}{3}} \qquad [2.7]$$

where ΔT is the temperature difference, ρ is the density, and the subscript w means that the values are evaluated at the wall. A and B are calibration constants that depend mildly on ΔT.

Much work in the area of measuring wall shear stress by using a heated thin-film gage has been done by Bellhouse and Schultz [9,10]. Bellhouse and Schultz calibrated a thin film probe to measure fluctuating skin friction.

The thermal method works if there is a relationship between the temperature gradient and the velocity gradient in the boundary layer at the wall. This method works only if the

Reynolds analogy holds for the flow being measured, and the flow is steady with a two-dimensional attached boundary layer.

The author calibrated a heat flux microsensor that was developed by Dr. T.E. Diller and Dr. S. Onishi [11] to measure skin friction in low speed subsonic flow. The heat flux microsensor is different than the heated film because the microsensor measures heat flux directly while the heated film just measures the electrical power necessary to keep the film at a constant temperature. The microsensor's basic principle of operation is it measures the temperature on either side of a known resistance by a series of thermocouples called a thermopile. The output from these thermopiles is directly proportional to the heat flux. Details of the calibration of the heat flux microsensor for skin friction measurements are included in Appendix A.

2.1.5 ELECTROCHEMICAL TECHNIQUES

The electrochemical technique or mass transfer probe works like the thin-film heated probe. The principle of operation is that the wall element is kept at a concentration different than that of the bulk fluid. The rate of mass transfer between the wall and the fluid is measured. The

element should be sufficiently small so that the concentration boundary layer δ_c lies within the linear portion of the boundary layer. The linear velocity distribution can be written U = Sy. Where S is the magnitude of the velocity gradient at the wall. For two-dimensional attached boundary flow, a relationship can be determined between the mass transfer rate and the velocity gradient S. If the fluid viscosity is known, then the wall shear stress is known since $\tau_w = \mu S$. Hanratty and Mitchell [12] showed that an analytical expression for the calibration can be derived, provided the following conditions are met:

1. The scalar boundary layer is within the region where U = Sy.
2. The flow is homogeneous over the surface of the element.
3. δ_c is small enough compared to the width, W, of the electrode so that the diffusion in the spanwise direction can be neglected.
4. Forced convection is large enough so that diffusion in the x-direction can be neglected.
5. Natural convection is small compared to forced convection.
6. The scalar boundary layer is small enough so that the influence of turbulent transport in the y-direction can be neglected.

Both the mass transfer and the heat transfer probes have advantages over the Stanton tube, Preston tube, and

sublayer fence in that they can be mounted flush with the wall and do not disturb the flow. The mass transfer probe has an advantage over the heat transfer probe in that calibration is not necessary. This is because the heat transfer probe experiences heat loss to the substrate that must be accounted for, and this problem does not occur with mass transfer techniques. A disadvantage of the mass transfer technique is it can only be used in liquid flow while the heat transfer probe can be used in both liquid and gaseous flows. Neither the mass transfer or the heat transfer probe has the ability of distinguishing reversed flow.

2.2 DIRECT METHODS

Direct methods for measuring skin friction have numerous advantages over indirect methods. The most important advantage is the skin friction is measured directly and no information about the flow field or the fluid properties is needed. There are; however, difficulties that arise with the implementation of direct methods for measuring skin friction. Winter [13] gave the following list of possible problems associated with direct measurement of skin friction:

1. Provision of a transducer for measuring small forces or deflections, and the compromise between the requirement to measure local properties and the

necessity of having an element of sufficient size that the force of it can be measured accurately.

2. The effect of the necessary gaps around the floating element.

3. The effects of misalignment of the floating element.

4. Forces arising from pressure gradients.

5. The effect of gravity or acceleration if the balance is to be used in a moving vehicle.

6. Effects of temperature changes.

7. Effects of heat transfer.

8. Use with boundary layer injection or suction.

9. Effects of leaks.

10. Protection of the measuring system against transient normal forces during starting and stopping in a supersonic tunnel.

Because of these problems that have to be overcome in the implementation of direct measuring skin friction devices, it is easier and cheaper to use indirect methods. Direct methods need to be used; however, when the flow field does not produce well defined boundary layers. Therefore, the three-dimensional, supersonic, combusting flows in SCRAM-jet combustors require direct measuring skin friction gages.

A floating element skin friction gage that was developed by Jim Putz [14] was designed initially for use in a SCRAM-jet combustor. Because of problems with temperature and normal

pressure sensitivity this gage had to be redesigned. The process that went into redesigning this gage is the topic of this thesis.

A cantilever type skin friction gage (Figure 2.3) was developed by Dianne Deturris [1] for use in SCRAM-jet combustors as well. This gage doesn't have the problems of temperature sensitivity that the floating element gage experienced because the strain sensing elements are removed from the flow and can be cooled. While this gage works well, it doesn't have the frequency response of the floating element skin friction gage. A skin friction gage with a high frequency response is needed in order to measure unsteady skin friction as well as skin friction presence in short-duration flows such as shock tubes.

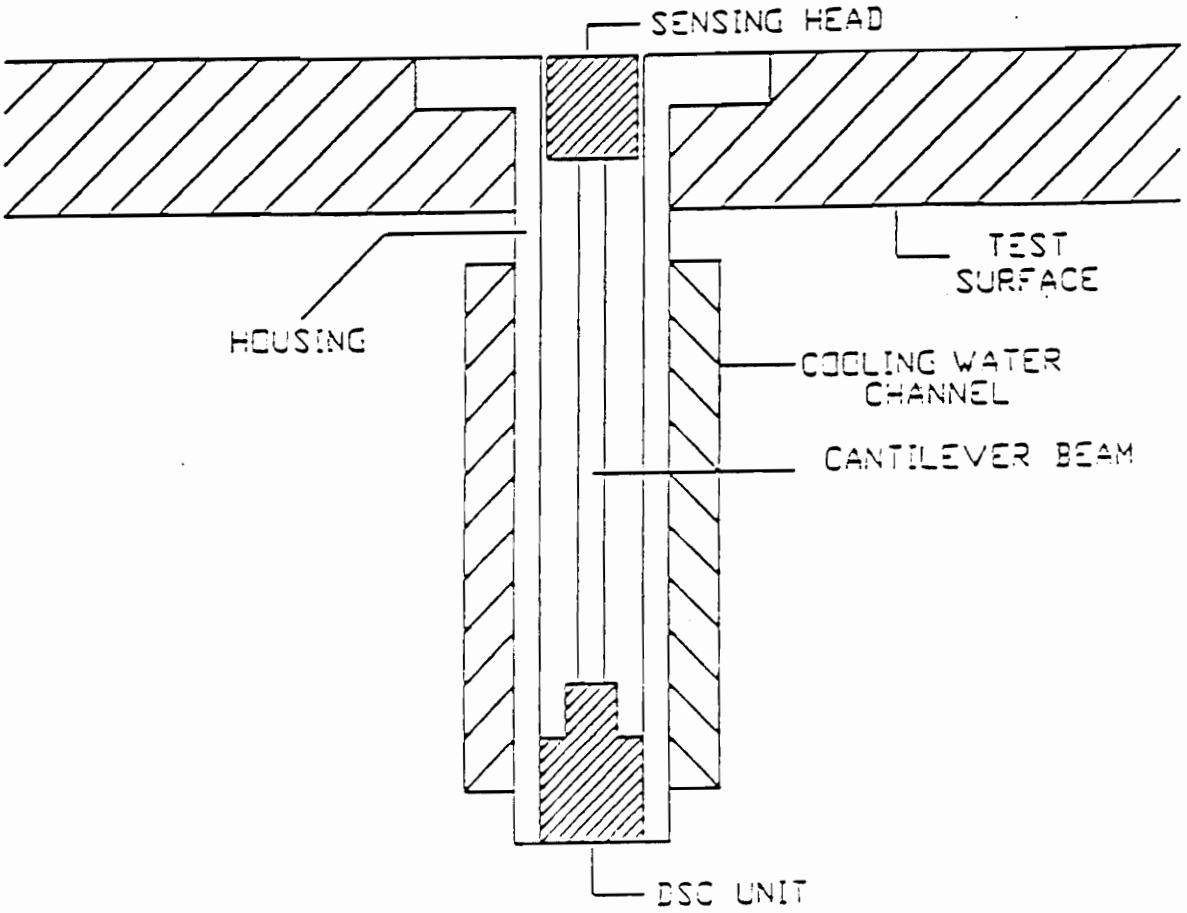

Figure 2.3 Cantilever type skin friction gage

Chapter 3

APPARATUS

3.1 DATA ACQUISITION

All of the skin friction gages that were designed, work with strain gages. In order to get an output voltage from the skin friction gage, the individual strain gages are wired into a Wheatstone bridge. This arrangement is designed to give a voltage output directly proportional to the skin friction.

The output from the Wheatstone bridge is amplified using a signal amplifier designed and built by John Putz [15]. Once the signal is amplified, it is captured on a Hewlett Packard dynamic signal analyzer. The signal can then be stored on a diskette and/or plotted on a graphics plotter.

3.2 STRAIN GAGE THEORY

The most prominently used type of strain gages are those that change electrical resistance with strain. Under this category fall two main types, the metallic wire or foil

resistance gages, and the semiconductor gages. Each type has advantages and disadvantages. The semiconductor strain gage has a much higher gage factor than the metal gages, but it also is much more temperature sensitive.

In Perry and Lissner's book The Strain Gage Primer [16] they list the ideal strain gage characteristics. The characteristics that they listed were:

1. The strain/resistance characteristics of the gage should be linear.

2. The gage should be small in size, easy to securely attach; its profile should be as low as possible so that it will respond in unison with the changes in the surface to which it is attached.

3. The gage should be highly sensitive in the direction of the expected strain while at the same time have minimum sensitivity to strains which are perpendicular to the primary sensing axis of the gage.

4. Stiffness in all directions should not be such that the stiffness of the test specimen is altered.

5. Calibrations should be simple and quick. Once done the calibration should remain stable with time, dynamic loading, and changes of temperature, pressure or humidity.

6. Frequency response should be high.

7. Remote indication and immersion in liquids should not present difficulties.

8. Gages should be inexpensive, reliable, and readily available. There should be a variety of types and sizes suited to a wide range of experimental situations.

In selecting a proper strain gage for the desired measurement, two primary factors must be considered. These two factors include operating temperature and state of strain including gradients, magnitude, and time dependence.

3.2.1 STATE OF STRAIN

In general strain gages can measure strain with a resolution of one microstrain. It is therefore desirable to have strain levels of 10 microstrain or more. All of the gage designs addressed here produce strain levels on the order of ten microstrain.

Once the strain level is known, the voltage output from the Wheatstone bridge can be determined. The relationship between the strain and the change in resistance of the strain gage is given by equation 3.1.

$$\frac{\Delta R}{R} = GFe \qquad [3.1]$$

Where ΔR is the change in resistance due to strain, R is the unstrained resistance of the gage, GF is the gage factor, and e is the Strain. Once the change in resistance due to strain is known, the Wheatstone bridge equations presented in the

next section can be used to determine the bridge output voltage. As shown in equation 3.1 the gage factor directly influences the change in resistance due to strain and therefore the gage output. Since the strain level is small, it is desirable to have the larger gage factor that semiconductor strain gages provide. While semiconductor strain gages are much more sensitive to temperature than metal gages, temperature compensation techniques make the usage of the semiconductor gages possible. Not only is the semiconductor strain gage is the best choice due to the strain magnitude, it also has a fast enough response for the intended dynamic signals.

3.2.2 OPERATING TEMPERATURE

The ideal strain gage would respond only to the strain that is to be measured. In reality; however, the strain sensitivity and resistivity of all known strain sensitive materials are temperature dependent. This means that the gage resistance as well as the gage factor will change with temperature.

When a strain gage is mounted to the test specimen, there are actually three factors that can lead to temperature caused

error. The first is that the gage resistance will change as the temperature changes. Table 3.1 shows how a batch of semiconductor strain gage resistances vary with changes in temperature. The second temperature effect is called temperature induced strain. This temperature induced strain occurs because of differences between the thermal expansion of the substrate material and the gage, and can be compensated by matching the thermal expansion coefficients of the gage and the substrate material. It should be noted that this compensation is only valid over a limited temperature range, because of the nonlinear character of both the coefficient of thermal expansion and the thermal coefficient of resistivity. The third reason that temperature induced error can occur is that the gage factor also varies as a function of temperature.

3.3 WHEATSTONE BRIDGE THEORY

The Wheatstone bridge (Figure 3.1) is the most commonly used circuit for measuring changes in resistance, because of its outstanding sensitivity and its ease of use. In Figure 3.1, E_{in} is the input voltage to the bridge, and E_{out} is the output voltage. The input voltage can be applied across any diagonal, while the output is to be measured across the opposite diagonal. When strain gages are placed next to each

Table 3.1 Temperature Dependance of Semiconductor Strain gages

Lot #	Gage #	Resistance at Temperatures		
		-40.0 °F	60.0 °F	160.0 °F
Lot 1	Gage 1	795.4	975.6	1209.1
	Gage 2	792.1	973.1	1207.2
	Gage 3	796.4	976.4	1209.6
	Gage 4	792.9	972.4	1205.1
Lot 2	Gage 1	805.2	988.0	1224.9
	Gage 2	802.4	984.1	1219.8
	Gage 3	806.4	989.7	1227.0
	Gage 4	802.1	983.9	1219.6
Lot 3	Gage 1	789.6	970.5	1203.8
	Gage 2	792.5	972.4	1205.1
	Gage 3	794.2	975.0	1208.2
	Gage 4	792.5	974.1	1208.5

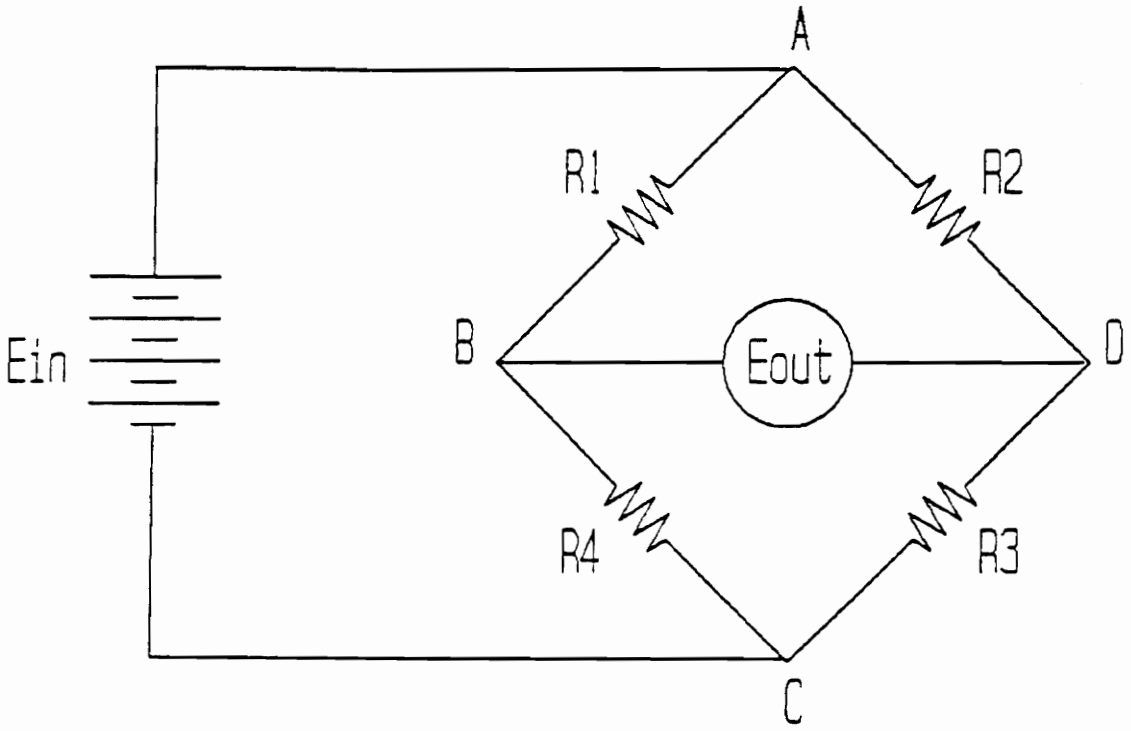

Figure 3.1 Basic Wheatstone Bridge Circuit

other in the circuit, the output from each gage is subtracted. And if the strain gages are placed opposite each other, their individual outputs add.

There are generally three different configurations of the Wheatstone bridge. The quarter-bridge configuration (Figure 3.2) is when only one arm of the Wheatstone bridge is an active strain gage and the other arms consist of bridge completion resisters or unstrained gages. The half-bridge configuration (Figure 3.3) exists when two arms of the Wheatstone bridge are active gages, and the full-bridge configuration (Figure 3.4) is operated with all four arms made up of active strain gages.

For the Wheatstone bridge configuration, the only resistor that should change value is that of the active strain gage, and only then as a function of strain. The output voltage is a function of E_{in}, R_1, R_2, R_3, and R_4. This relationship is given in equation 3.2.

$$E_{out}=E_{in}\left(\frac{R_1R_3-R_2R_4}{(R_2+R_4)\,(R_2+R_3)}\right) \quad [3.2]$$

This relationship can be seen if the two sides of the bridge in Fig 3.1 are treated as individual voltage dividers

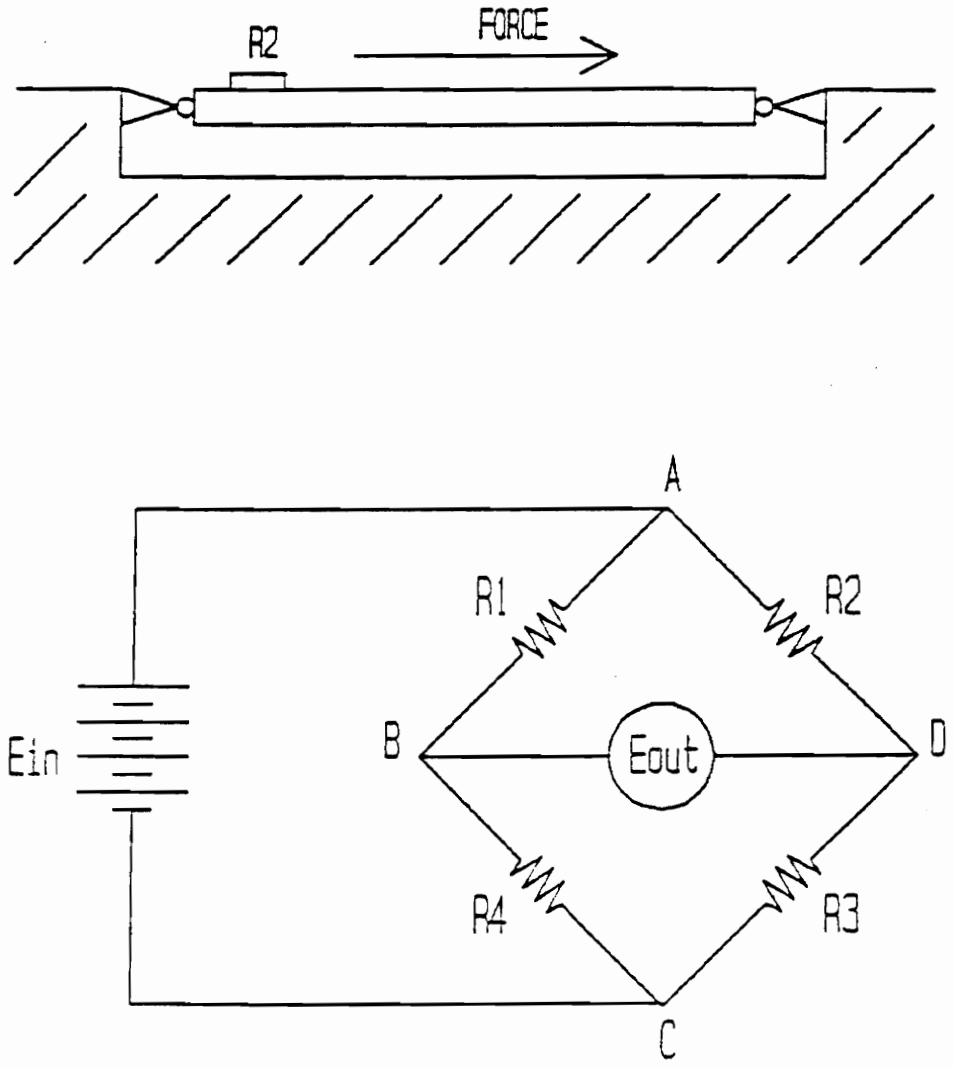

Figure 3.2 Wheatstone Quarter-Bridge Circuit

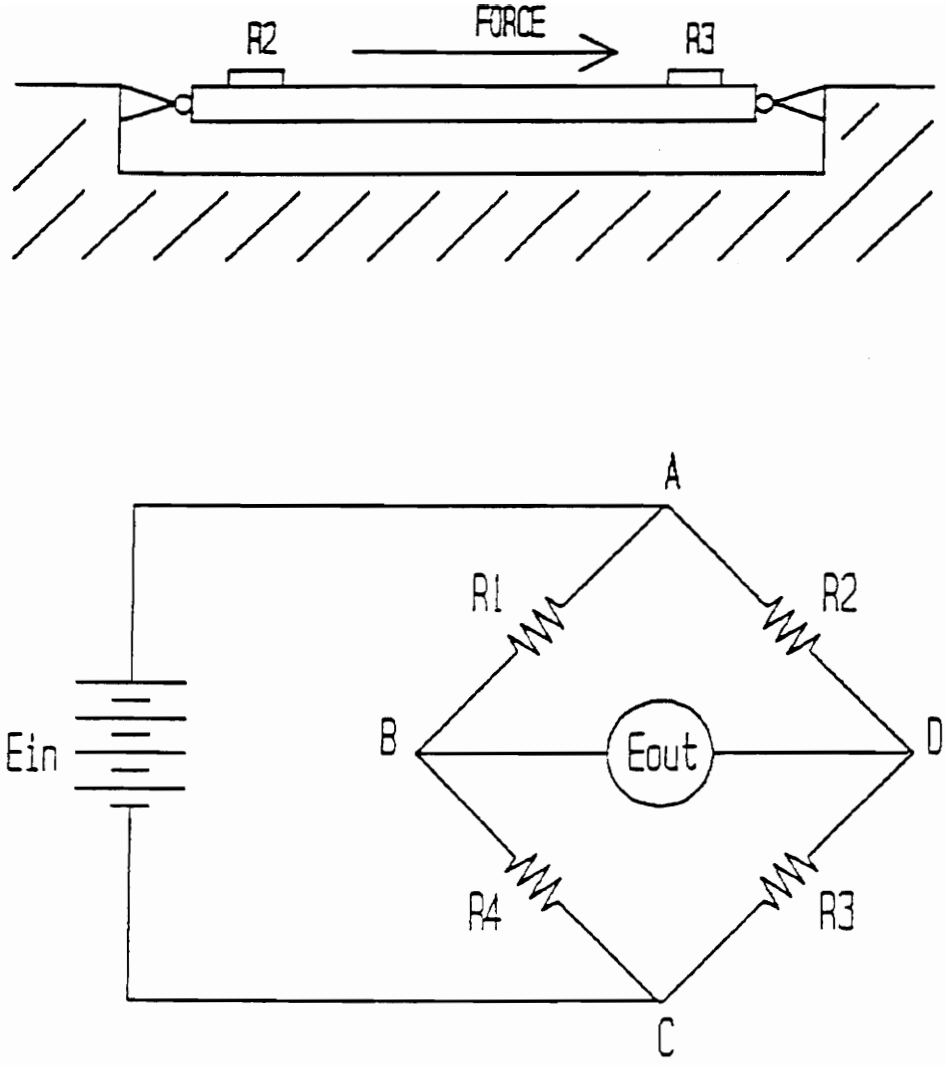

Figure 3.3 Wheatstone Half-Bridge Circuit

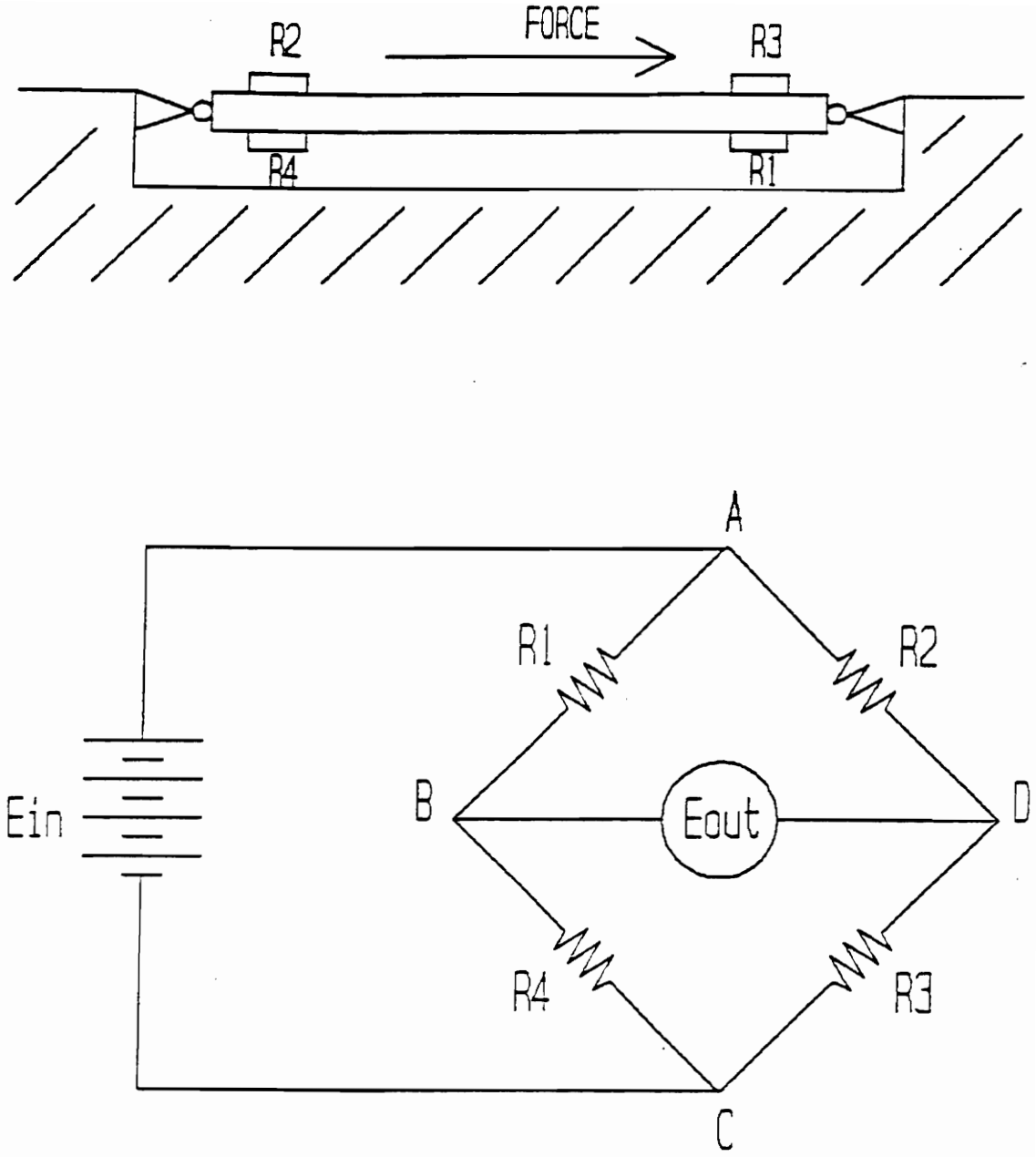

Figure 3.4 Wheatstone Full-Bridge Circuit

$$E_{AB}=E_{in}\left(\frac{R_1}{R_2+R_4}\right) \qquad [3.3]$$

and

$$E_{AD}=E_{in}\left(\frac{R_2}{R_2+R_3}\right) \qquad [3.4]$$

from the voltage potentials E_{AB} and E_{AD}, the bridge output is equal to equation 3.5.

$$E_{out}=E_{AB}-E_{AD} \qquad [3.5]$$

and if you substitute equations 3.3 and 3.4 into 3.5 and simplify the result is equation 3.2. Looking at equation 3.2, it is clear to see that the condition for the bridge to be balanced is equation 3.6.

$$R_1R_3=R_2R_4 \qquad [3.6]$$

It is very uncommon that the resistors match up exactly so that the bridge is balanced. That is why most Wheatstone bridge circuits have a built in bridge balance method. Starting measurements from a balanced bridge makes measuring small outputs much easier than if the measurement was started with a large voltage base.

Making measurements in the quarter-bridge circuit (Fig. 3.2) allows the output of the Wheatstone bridge to be due only to changes in resistance of the one active strain gage. This is the best choice if it is uncertain what is going on with the individual strain gages. A major disadvantage with the quarter bridge circuit is that it is more temperature sensitive than the half and full-bridge circuits.

Another disadvantage of the quarter-bridge circuit is the possibility of nonlinear output. The half and full bridge configurations can avoid nonlinear output by proper positioning of gages on the test specimen and in the bridge circuit. The nonlinearity of the quarter-bridge circuit can be seen by the relationship between the change in resistance of the gage and the bridge output voltage given by equation 3.7.

$$\Delta E_{out}=E_{in}\left[\frac{(\Delta R_2/R_2)}{4}\left(\frac{-2}{2+(\Delta R_2/R_2)}\right)\right] \qquad [3.7]$$

The term $2/(2+(\Delta R_2/R_2))$ is the term that contributes to the nonlinear output. From this nonlinear term it can be shown that tensile strains give an output less than what it should be while compressive strains produce an output too large.

There is a correction factor that can be used to compensate for bridge nonlinearity in the quarter bridge circuit. The correction factor is given by equation 3.8.

$$CF = \frac{(\Delta R_2/R_2)^2}{8+4(\Delta R_2/R_2)} \qquad [3.8]$$

A half-bridge circuit (Fig. 3.3) has advantages over the quarter bridge in that it is less temperature sensitive and the output due to strain is doubled. The temperature compensation is achieved by placing the gages next to each other in the Wheatstone bridge circuit. With the gages next to each other, their outputs subtract. The output of the strain gages due to temperature is the same for both gages, provided they have the same characteristics and they both are exposed to the same temperature. If the gage placement is chosen so that one gage sees a positive strain, and the other sees a negative strain of the same magnitude, then when the gage outputs are subtracted, the output due to strain is doubled, while the output due to temperature is canceled. This configuration can lead to measurement error; however, if the individual strain gages don't exactly see the same temperature, or if the strain fields don't see the same magnitude.

Another major advantage of the half-bridge circuit is the elimination of the nonlinear output of the Wheatstone bridge. With the gage placement on the test specimen and in the bridge circuit as shown in Fig. 3.3, the output of the half-bridge circuit is given by equation 3.9.

$$\Delta E_{out} = \frac{E_{in}}{2} \frac{\Delta R}{R} \qquad [3.9]$$

Where R is the resistance of both gages and ΔR is the change in resistance of both gages.

The full bridge configuration has the temperature compensation of the half-bridge, but its output due to strain is twice that of the half-bridge. With four active gages of resistance, R, configured as shown in Figure 3.4, the output voltage of the full bridge is given by equation 3.10.

$$\Delta E_{out} = E_{in} \frac{\Delta R}{R} \qquad [3.10]$$

3.4 SKIN FRICTION GAGE CALIBRATION

3.4.1 CONVENTIONAL METHOD

The conventional method of calibrating direct force skin friction gages is to load them statically with weights and record the corresponding voltage output. This can be done by attaching a string to the center of the gage surface and hanging weights from the string to load it. The calibration can use either a pulley system with the gage positioned vertically or the gage positioned horizontally while hanging weights on the string without using a pulley.

Table 3.2 gives the results of a typical gage calibration. The skin friction is determined by taking the weight that is hung from the string multiplied by gravity and then divided by the area of the active gage surface as given by equation 3.11.

$$\tau_w = \frac{mg}{A_s} \qquad [3.11]$$

Once the data is obtained from a calibration, a relationship can be established between the gage output and the skin friction. A linear regression can be made to the

Table 3.2 Sample Calibration data

WEIGHT	T_w (Pa)	ΔE_{out} (V)
2 grams	68.8	0.094
5 grams	172.1	0.251
10 grams	344.2	0.475
20 grams	688.4	0.997
50 grams	1720.9	2.436

data to get an equation relating voltage output to skin friction. Figure 3.5 shows a graph of the calibration given in Table 3.2. The symbols correspond to the individual data points, and the line represents the linear regression given by equation 3.12.

$$\tau_w = -1.0 + 705(E_{out}) \qquad [3.12]$$

3.4.2 CALIBRATION BY THE VISCOMETER

Another way to load the gage for calibration purposes is by a viscometer. The viscometer used was designed and built by Rodney Bowersox [17] for the purpose of calibrating the sputtered skin friction gage. A sketch of the viscometer is provided by Figure 3.6. The rotating disk is placed in a drill press or milling machine. The gage to be calibrated is then placed flush with the surface of the base. The fluid retaining ring is bolted down to keep the viscous fluid in place. Once the viscometer is set up for calibrating, viscous fluid is placed inside the retaining ring, and the calibration can be made.

The viscometer operation is really very simple. The gage to be calibrated is placed far away from the center of the rotating disk. This allows the assumption that the flow is

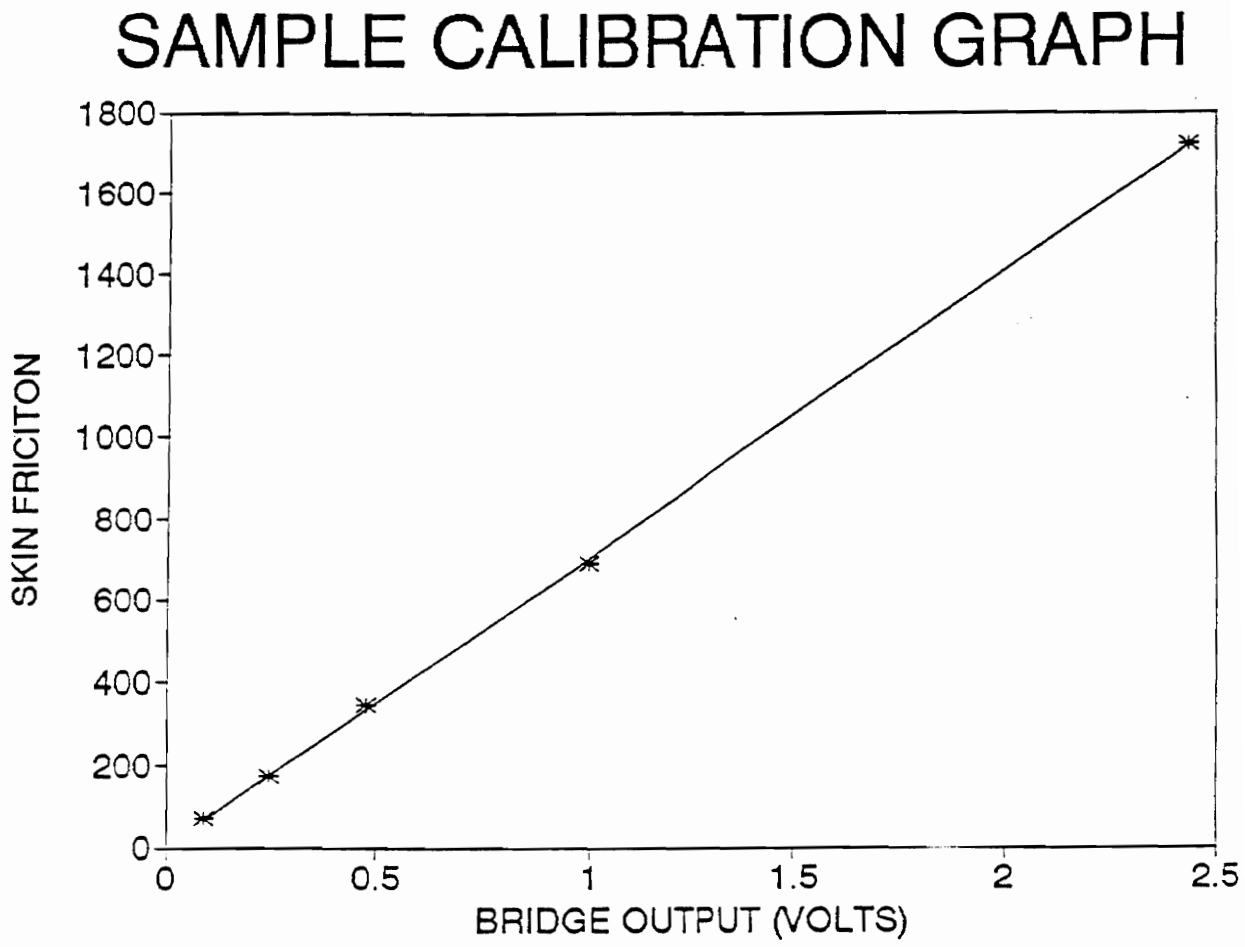

Figure 3.5 Graph of Skin Friction Gage Calibration

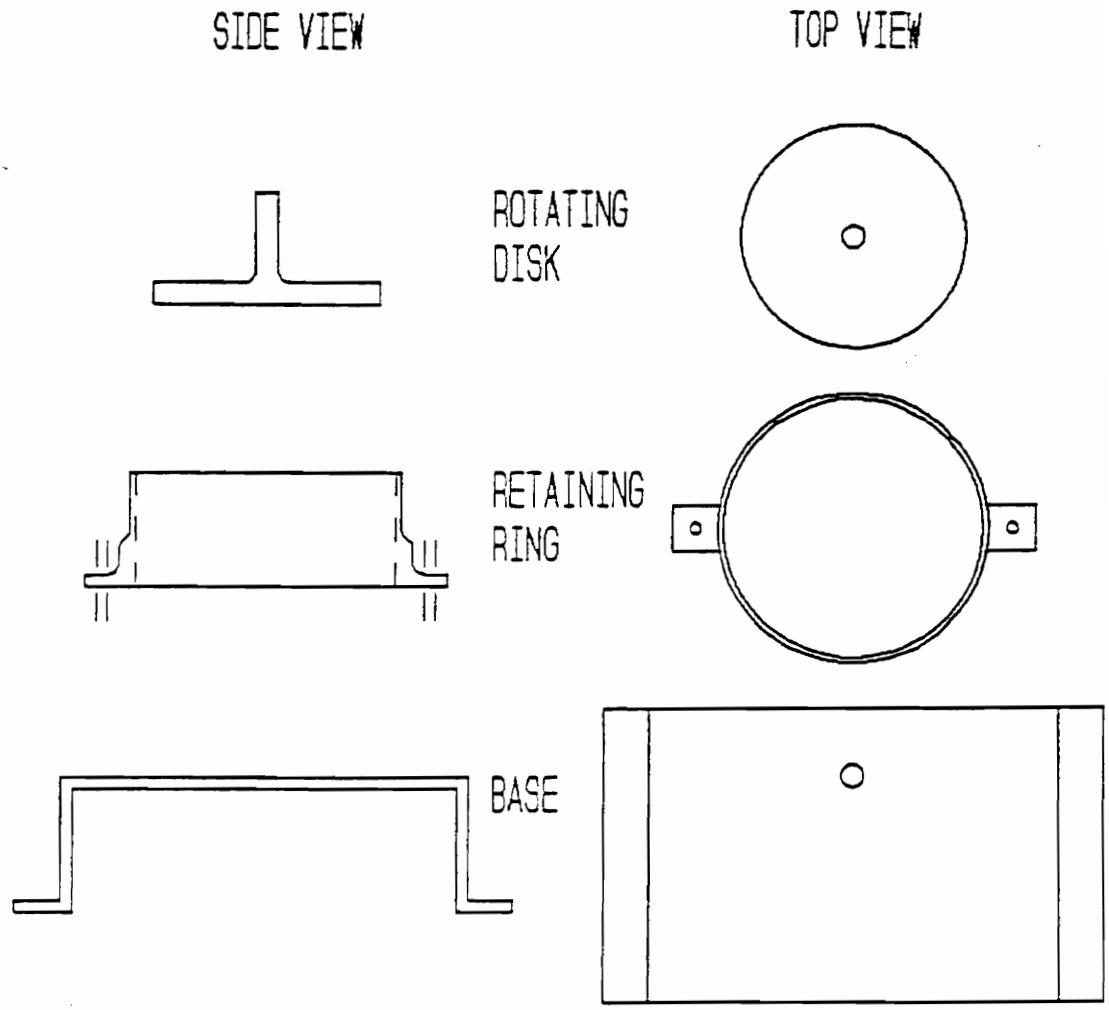

Figure 3.6 Sketch of Viscometer Used For Gage Calibration

one-dimensional to be made. Using the further assumptions that the flow is steady and that viscous dissipation heating effects are negligible, the Navier-Stokes equation for the flow reduces to equation 3.13.

$$\nu \frac{d^2u}{d^2y}=0 \qquad [3.13]$$

Applying the boundary condition that u=o, at y=o and u=ωr, at y=h, equation 3.13 can be solved for the velocity distribution, equation 3.14.

$$u=\frac{\omega r}{h}y \qquad [3.14]$$

The skin friction, τ_w, is related to the velocity distribution via equation 3.15.

$$\tau_w=\mu\left(\frac{\partial u}{\partial y}\right)_{y=0} \qquad [3.15]$$

Equations 3.14 and 3.15 can be solved for the skin friction, τ_w, as a function of angular velocity, ω, distance from the center of rotation, r, height of fluid, h, and fluid viscosity, ν. This relationship is given by equation 3.16.

$$\tau_w=\mu\frac{\omega r}{h} \qquad [3.16]$$

For calibration of the skin friction gages, silicon oil (with a viscosity of 200 centistoke) was chosen as the viscous fluid. Table 3.3 shows what skin friction, τ_w, is given for various angular velocities. The height of the fluid h is fixed at 40 thousandths of an inch and the radius is fixed at 2.5 inches and the fluid viscosity is 200 centistoke.

3.5 MACH 3 SUPERSONIC TUNNEL

To test the skin friction gages in high speed flow, the supersonic tunnel at Virginia Polytechnic Institute and State University was used. This facility belongs to the Aerospace department and it works as a blowdown facility.

For test purposes, a Mach 3 nozzle was used. A compressor is used to pump air into a storage tank at high pressure. Once the tank reaches 300 psi it is ready for blowdown into the supersonic nozzle. During blowdown a Mach 3 flow is sustained for approximately 15 seconds. The total pressure in the tunnel is regulated at approximately 95 psi.

A problem that was encountered with this tunnel was the static pressure. The static pressure in the section is approximately 2 psi. The skin friction gage is mounted on the

Table 3.3 Skin Friction versus angular velocity

RPM	T_w (Pa)
100	124.4
200	248.7
300	373.1
400	497.4
500	621.75

gage body, which in turn is inserted into a test plate flush with the tunnel wall. With this configuration the gage body is exposed to atmospheric pressure outside of the tunnel, but inside the test section the static pressure is 2 psi. This pressure difference creates a normal pressure on the active element of the skin friction gage. This normal pressure is a source of measurement error. To eliminate the normal pressure effects, the skin friction gages were tested in a Free-Jet Facility designed to operate with atmospheric static pressure.

3.6 FREE JET FACILITY

The Free-Jet Facility was designed and built by John Mills [18] for the purpose of testing injection of gas into a supersonic cross flow. This free jet was designed to operate at Mach 1.95. Because the flow is supersonic and comparable to the larger supersonic tunnel, the Free-Jet Facility provided another viable avenue for skin friction gage testing.

This Free-Jet Facility had several advantages over the large supersonic tunnel. It is easier to set up and to run tests with. Also because the Free-Jet Facility is smaller than the supersonic tunnel, the flow can be sustained for a much longer period of time, and it is possible to make several

short runs without losing pressure in the tanks. This feature shortens the time necessary to make successive skin friction tests.

Figure 3.7 provides a schematic of the Free-Jet Facility that was used to test the skin friction gages. A test plate was mounted along one of the walls of the exit nozzle, and the measurements were taken as air at Mach 1.95 exited the nozzle. Calculations were done to compute the expected shear stress from this flow. These calculations included in Appendix B, demonstrated that the skin friction is approximately 500 Pascal with a C_f of 0.002.

3.7 SHOCK TUBE

The supersonic tunnel and the Free-Jet Facility are good for testing the skin friction gages, but since the research is aimed toward making skin friction measurements in shock tubes, a shock tube was designed an built by Yagnavulkya Mukkamala [19].

This shock tube was built to study the transient responses of skin friction and heat flux gages to short-duration, high-speed flows. It is made out of three and one-

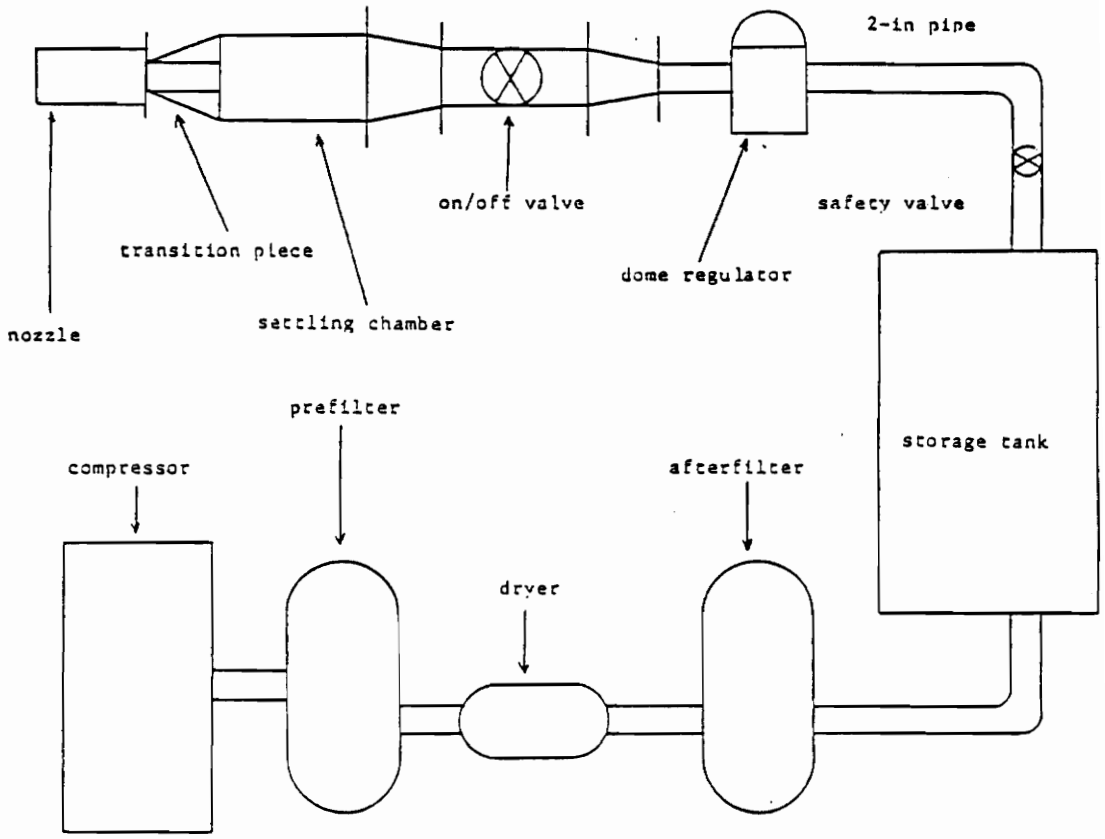

Figure 3.7 Sketch of the Free-Jet Facility

quarter inside diameter pipe. The driver section of the shock tube is eleven and one-half feet long, and the driven low pressure side is fifteen feet long. Mukkamala chose these lengths so that the flow duration would be approximately five milliseconds, neglecting viscous and other damping effects. The end of the low-pressure, driven section was fitted with a Mach 2 nozzle with an exit to throat area ratio of 1.67.

The driver and low pressure sections of the shock tube are separated by a mylar diaphragm. The driver section is then filled with compressed helium, which serves as the driving gas. Helium was chosen for its shock-attenuation resisting characteristics. Once the driver section reaches the desired operating pressure, the diaphragm is ruptured by a hot-wire grid made of two pieces of 5 mil thick Nickel-Chromium wire, burnt down by a 20 volt, 1.5 ampere current from a DC power supply.

The skin friction gage is positioned in a test plate along one of the walls of the nozzle exit. In order to capture the signal from the skin friction gage the signal analyzer had to be triggered. The signal analyzer was set to pre-trigger and post-trigger for the amount of data points necessary to capture the full signal.

Chapter 4

GAGE DESIGN PROCESS

The objective of this research is to develop a gage that can measure skin friction in high-speed, short-duration flows. The gage should have a fast response time so it can make measurements in the millisecond time range. This chapter traces the gage design process from original design to present stage, while presenting the rationale behind each new design.

4.1 ORIGINAL GAGE DESIGN

The skin friction gage that was originally tested was a gage developed by Jim Putz [13]. This gage, shown in Figure 4.1, uses a floating element concept. A 1 cm square is laser cut into a 5 mil thick sheet of stainless steel, and the corners are left attached as shown in the figure. Strain gages are placed on the corners and wired into a Wheatstone bridge configuration in order to get a voltage output directly proportional to the skin friction. Figure 4.2 shows an assembly drawing of this skin friction gage design. The laser cut thin film is spot welded to the mounting head. Oil is placed behind the laser cut thin film and then held in place

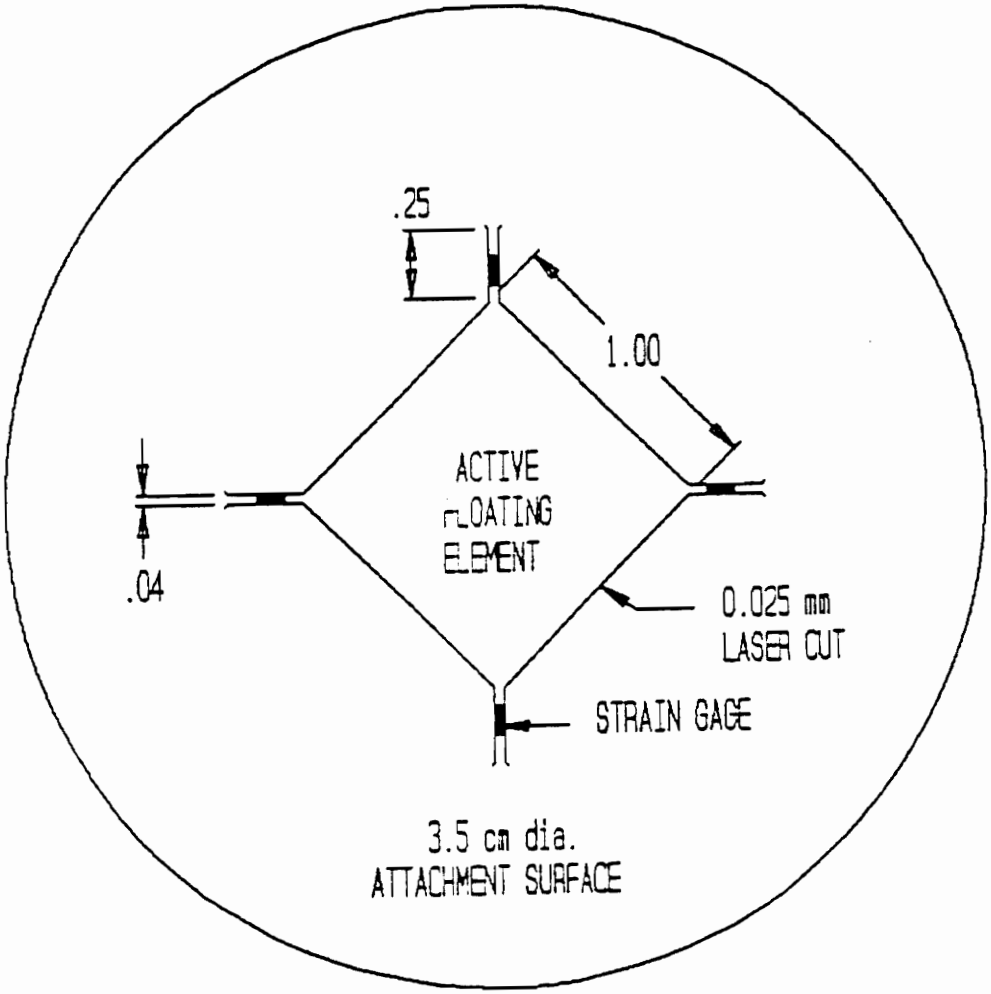

Figure 4.1 Laser cut thin-film

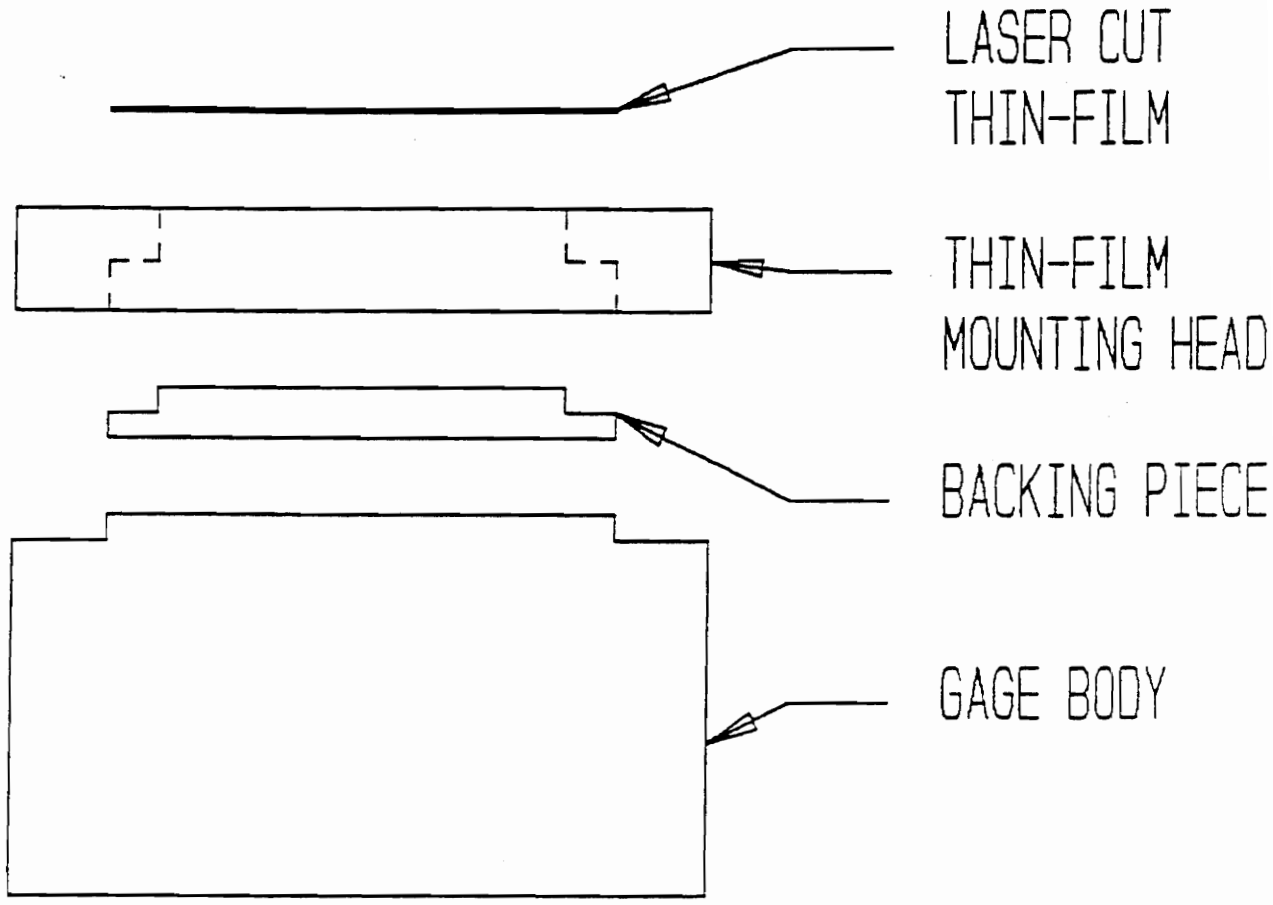

Figure 4.2 Assembly drawing of original gage design

by a backing piece. Next the whole unit of the mounting head and backing piece together are screwed on to the gage body.

When flow passes over one of the diagonals of the floating element, the strain gage at the leading edge is in tension while the strain gage at the trailing edge is in compression. These two gages can be wired into a Wheatstone half-bridge configuration, so that the outputs subtract and temperature and bending compensation is achieved, provided both gages experience the same temperature and the same bending due to normal pressure.

A larger model of this gage design worked well in subsonic flow [13]. When this particular gage design was tested in supersonic flow; however, several problems were encountered. The testing of this original gage was first done in the supersonic Mach 3 tunnel. The calibration of this gage prior to testing showed that the gage was performing as expected. The gage output from the test was on the order of 2 Volts, one hundred times larger than the expected output of 20 mV. The next step in the gage design process was to determine the problem and change the design.

As the Mach 3 tunnel test was in progress the gage could be observed, and it appeared that the laser cut thin film was

being sucked up into the flow. It was hypothesized that a large normal pressure was being exerted on the gage, and that the stress in the tabs due to bending was not being compensated for adequately. To test whether bending due to normal pressure was causing measurement error, the gage was placed in a vacuum to simulate the normal pressure experienced by the gage in the Mach 3 tunnel. This Vacuum test gave an output on the order of one volt. The gage was designed to yield zero output due to normal forces. This test demonstrated that normal pressure was indeed a factor leading to measurement error.

Once normal pressure was determined to be a source of measurement error in the supersonic tunnel, the gage was tested in the Free-Jet Facility where the static pressure is atmospheric. Because of the atmospheric static pressure, the bending of the tabs due to normal pressure should not occur. The gage output from this test was still on the order of one volt. This measurement error was hypothesized to be due inadequate temperature compensation. To test whether temperature compensation was indeed a source of measurement error, the skin friction gage was placed, unstrained, into an oven. The oven was then heated to determine if temperature compensation was achieved. The gage output should be zero, but was on the order of hundreds of mV. This oven test showed

that inadequate temperature compensation was another source of measurement error.

From the oven and vacuum tests it was shown that the pressure and temperature compensation techniques as implemented were not adequate. The output due to temperature and bending error combined were on the order of one hundred times the output that is expected from the skin friction. In order to make this gage design work in high speed, high temperature flow, the output due to the temperature effects and normal pressure effects have to be minimized.

4.2 MINIMIZING PRESSURE EFFECTS

The output due to pressure effects was caused by nonuniform bending in the tabs. If the individual tabs experienced the same bending stress, the Wheatstone bridge configuration would yield zero output. The gage was intended to work this way, but because the 5 mil thick stainless steel sheet does not act as a rigid body, nonuniform bending occurs in the tabs. This output due to pressure effects can be minimized by either of three ways. (1) Make the floating element act as a rigid body so that there is uniform bending in the tabs (2) restrict the movement of the tabs so that

there is no bending in the tabs at all, or (3) compensated locally for the bending in each tab.

4.2.1 MINIMIZING PRESSURE EFFECTS BY ELIMINATION OF BENDING IN THE TABS

In order to prevent the tabs from bending, the oil that was placed behind the thin film was replaced by silicon rubber. The idea being that the silicon rubber is weak enough in shear to still allow the strain gage to measure the shear forces, but strong enough to prevent the tabs from bending normally. This modification, made to help eliminate the pressure effects, also led to the sputtered skin friction gage concept addressed in section 4.5. This new method of using silicon rubber instead of oil, decreased the sensitivity to normal forces by approximately ten times. Even with this new gage modification, the signals that were being measured were too large to be skin friction. Either the nonuniform bending needed to be further minimized or temperature effects had to be compensated for.

4.2.2 MINIMIZING PRESSURE EFFECTS BY LOCAL COMPENSATION

Another gage modification included an attempt to compensate locally for the bending effects. This gage called the top-bottom gage, got its name from the strain gage placements. A strain gage was placed on the top and the bottom of each tab, and wired into a Wheatstone bridge so that the localized bending at each tab was compensated (Figure 4.3). This gage also had some temperature compensation because of the insulation layer that had to be used to cover the top gages. The top-bottom gage was vacuum tested and determined to decrease the normal pressure effects by a factor of approximately ten times. While this was an improvement, the output due to pressure effects would still be on the order of 100 mV, but the output due to skin friction is only on the order of ten mV.

4.3 TEMPERATURE COMPENSATION

In the original gage design, temperature compensation occurred in the half-bridge circuit only if both active strain gages saw the exact same temperature. Small differences in

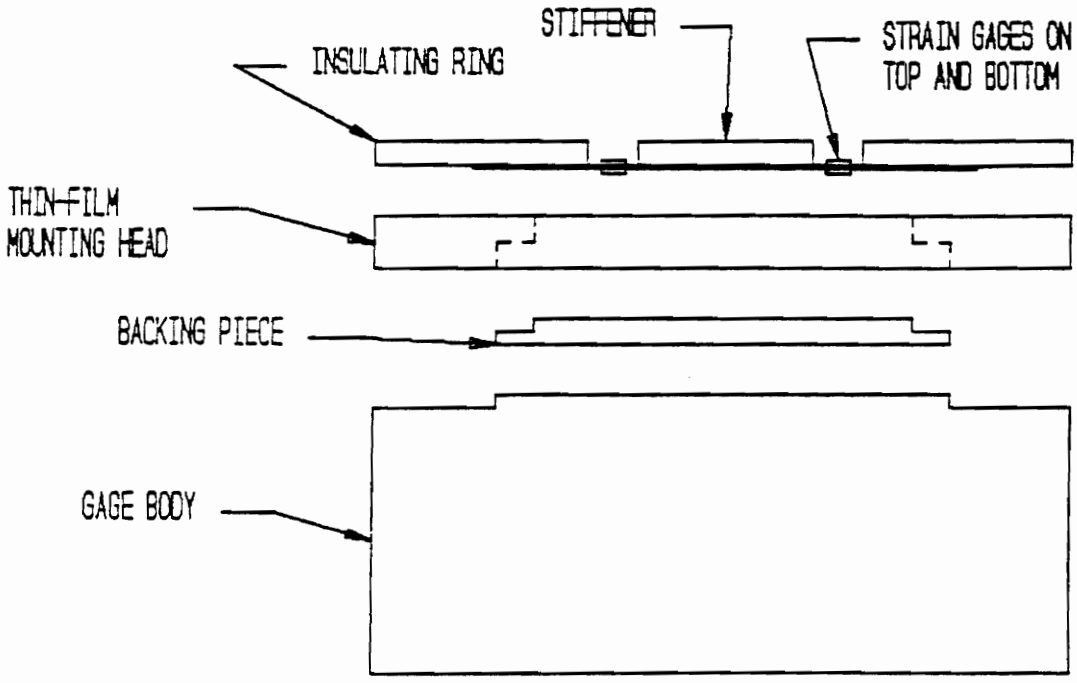

Figure 4.3 Assembly drawing of Top-Bottom gage design

temperature between the gages to be compensated can lead to a rather large error. The error occurs because piezzo-resistive gages are very sensitive to temperature. There were two methods of temperature compensation that were used with the current gage design. (1) Insulate the gage so that the temperature change of the strain gage is minimal over the time of the test, and (2) actively compensate for the temperature at each individual tab.

4.3.1 TEMPERATURE COMPENSATION BY INSULATION

The individual strain gages were insulated from temperature changes by placing a material with low thermal conductivity over the metal laser cut film, with a cut out stiffener piece placed over the active element as shown in Figure 4.4. Because the time length of the measurements that are to be made are small (in the millisecond time range), the gage can be designed so that the measurement will be taken and completed before the temperature effects reach the strain gages.

$$t=\frac{\delta^2}{16\alpha} \qquad [4.1]$$

Equation 4.1 gives the design relationship for the insulating

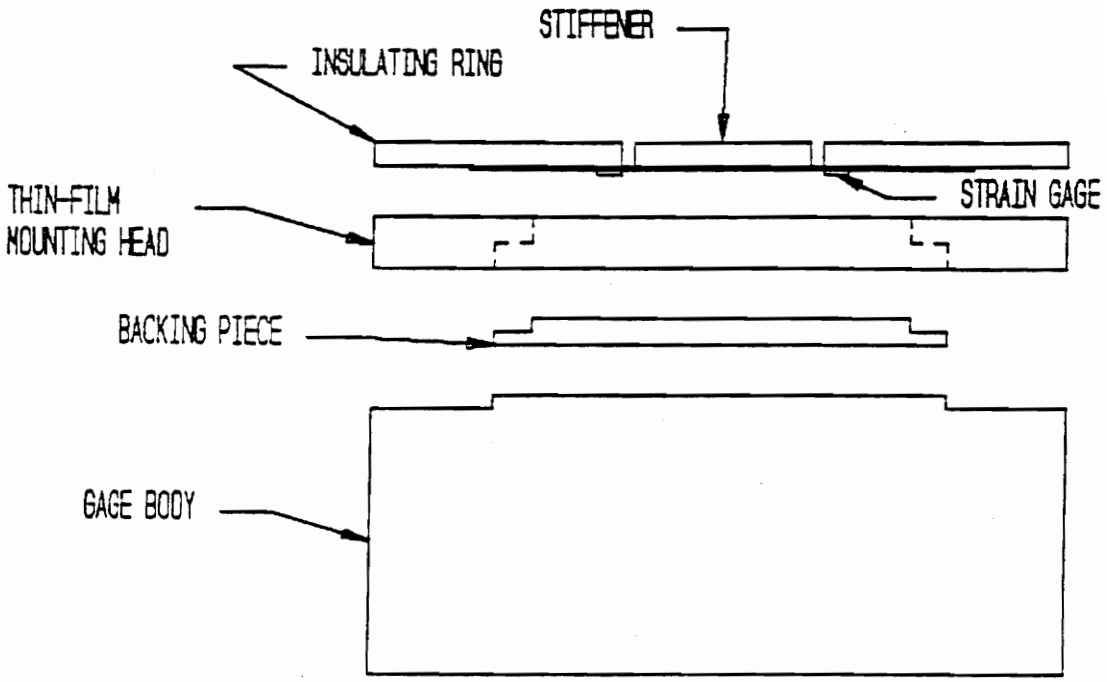

Figure 4.4 Temperature compensation by insulation ring

ring, assuming a semi-infinite conduction model. Delta is the thickness of the insulating ring, and alpha is the thermal diffusivity of the insulating material. In order for the gage to be insulated from temperature effects, a material had to be chosen with the right thermal diffusivity and made to the proper thickness. For this gage design, plexiglass was chosen as the insulator. The plexiglass was made one-eighth inch thick and it has an alpha of 7.5×10^{-7} meters squared per sec. These properties give a time of 0.84 seconds for the temperature effects to reach the gage.

This design was implemented and then tested with a heat gun. The tests were run by letting the heat gun reach operating temperature and then quickly passing it over the surface of the gage. The output from the gage was monitored to see when the temperature effects first appeared. This test showed promise in that there appeared to be time lag between the heat applied and the change in gage output. This time lag was difficult to quantify because it was not clear exactly when the heat was applied versus when the gage's output changed due to the temperature effects.

With the promise of temperature compensation for a short time span, this new gage design was tested in the Free-Jet

Facility. The static calibration of this gage design determined that the gage should produce a signal of approximately 20 mV for the skin friction expected from the Free-Jet Facility. When the tests where run in the Free-Jet Facility the gage produced a signal on the order of a hundred mV. If skin friction were actually being measured, the gage output would be the same magnitude but different signs when the gage was rotated 180 degrees. This was not the case with these tests. The magnitude of the gage output varied, sometimes by hundreds of mV, and the gage output did not change signs.

4.3.2 TEMPERATURE COMPENSATION LOCALLY AT EACH TAB

This design used two strain gages at each tab. One strain gage was placed on the tab so that it would feel the temperature effects as well as the strain due to the shear force. The other strain gage was placed as close to the first gage as possible without being on the tab so that the only output from that gage would be due to temperature effects (Figure 4.5). The gages were then wired into a Wheatstone bridge configuration so that the signals would subtract. Since both gages are close to each other, they should see the

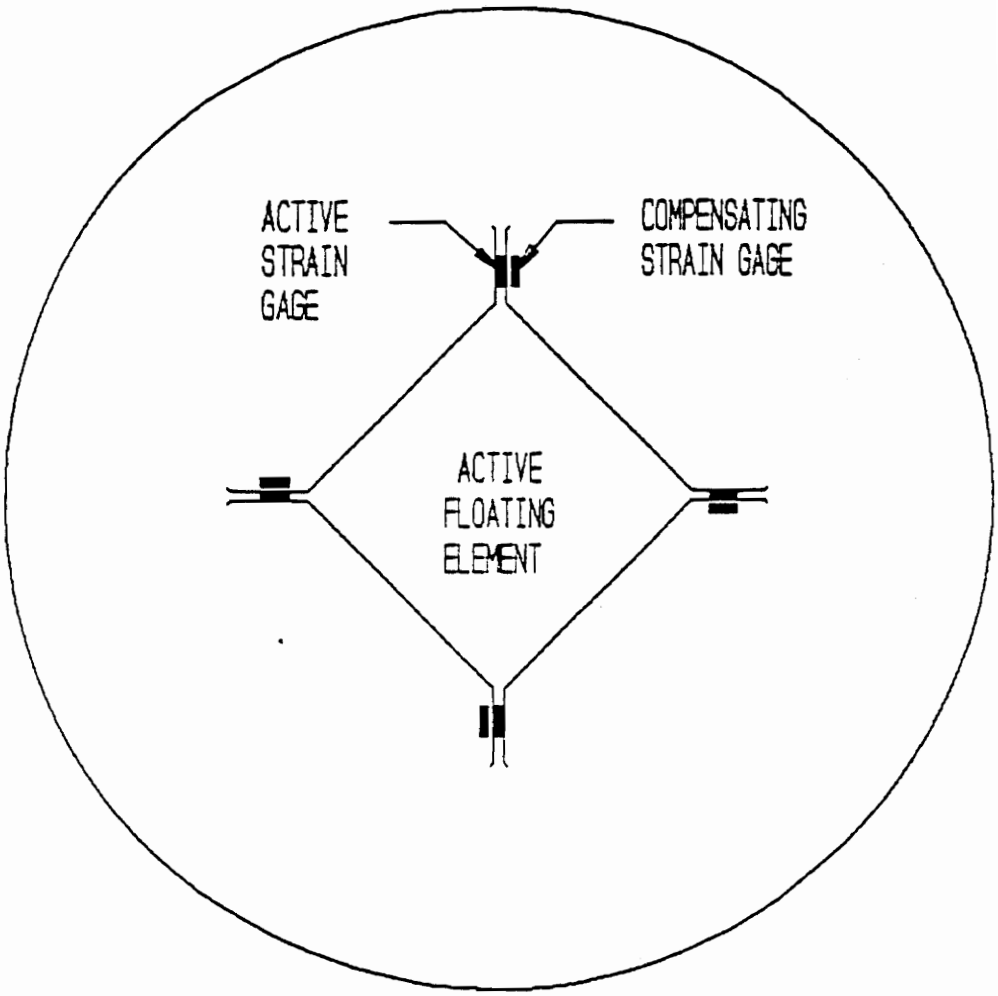

Figure 4.5 Temperature compensation (Locally at each tab)

same temperature, and thus the output due to temperature would be the same and the Wheatstone bridge would output a signal only due to strain.

This gage design was tested with the heat gun and in the Free-Jet Facility. As before, it was not evident from the heat gun tests how well the temperature effects were compensated. The Free-Jet Facility tests were similar to the previous gage design tests. The signals were on the order of ten times larger than the expected output from the static calibration. The magnitude varied and the gage output did not change signs when the gage was rotated 180 degrees.

4.4 RESULTS OF PRESSURE AND TEMPERATURE COMPENSATION

In order to keep the various gage designs straight, Table 4.1 lists all of the gage designs presented thus far, and also what the designs were to accomplish. All of these pressure and temperature compensation designs were implemented, but none of them were able to measure skin friction accurately.

The bending and temperature compensation attempts reduced the gage output due to temperature and bending, but the

Table 4.1 Gage design classifications

GAGE NAME	SPECIAL FUNCTION
ORIGINAL GAGE	ORIGINAL GAGE DESIGN
SILICON BACKED GAGE	MINIMIZE PRESSURE EFFECTS
TOP BOTTOM GAGE	MINIMIZE PRESSURE EFFECTS
INSULATED GAGE	MINIMIZE TEMPERATURE EFFECTS
LOCAL COMPENSATION GAGE	MINIMIZE TEMPERATURE EFFECTS

compensation was not adequate. The bending and temperature effects can produce a signal up to one hundred times the expected gage output due to skin friction. Even if the output due to bending and temperature effects are reduced, it can still be larger than the signal due to skin friction.

Further tests were done and it was determined that all of the gage designs presented so far would give a large output with any type of distortion. When a C-clamp was tightened against the gage body, strain fields were produced in the thin film, which in turn produced a large output from the Wheatstone bridge. The output was so large that the amplifier output was saturated at 7 Volts. Because the thin film is spot-welded onto the mounted head, strain fields can be transferred right from the gage body into the thin film. It was also shown that temperature effects occurred not only when the strain gages experienced a change in temperature, but changes in temperature also produced thermal strain which gives inaccurate output as well.

Because of this new reason for measurement error, the current skin friction gage designs had to be modified. The research here went in two directions. One was the sputtered gage which was mentioned before, and the other the T-top gage design, which was designed to eliminate temperature and

pressure effects as well as the distortion problem. These two gages are presented in the next sections as well as some results of testing.

4.5 SPUTTERED SKIN FRICTION GAGE

The bending compensation method of putting silicon rubber beneath the thin film, led to the development of the sputtered skin friction gage (Figure 4.6). This gage works on a different concept than the original gage design. The original gage design uses a floating element with strain concentrations where the strain gages are mounted. The sputtered skin friction gage, unlike the original gage design, has no gaps and the strain that is measured is the differential strain across the strain gage itself. The basic concept of the sputtered gage is that a strain gage is attached at one end to a stiff base and the remainder of the strain gage to a weaker material. When a shearing force is applied to the surface, the weak material will shear relative to the base and will cause the strain gage to experience this differential strain.

For the sputtered design, a 5 mil deep groove is cut into an aluminum nitride disk. The groove is then filled with silicon rubber and allowed to cure. Strain gage patterns are

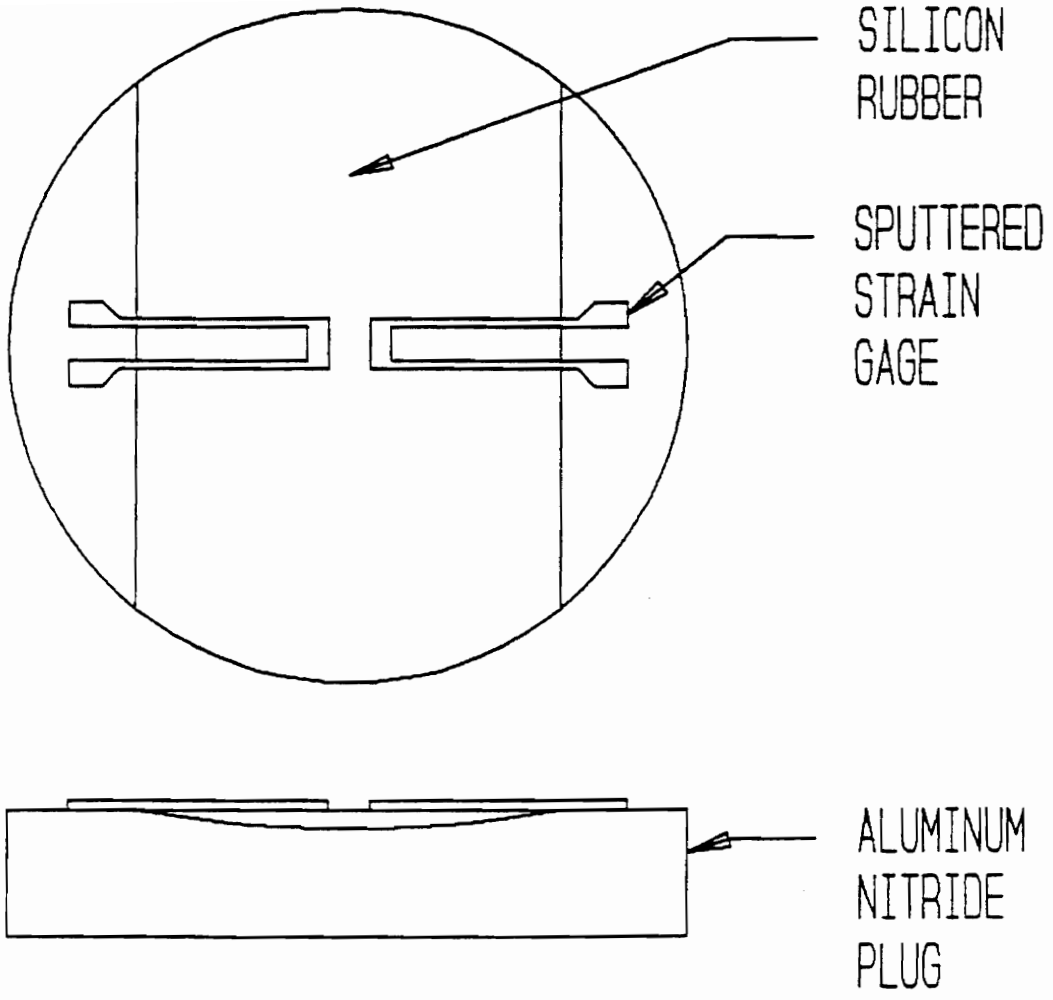

Figure 4.6 Sketch of Sputtered Skin Friction Gage

then sputtered on top, with most of the strain gage on top of the silicon. Because of this groove geometry, the strain would be zero right at the intersection and would increase as the center of the groove is approached. The center would be the point of highest strain, and then the strain would decrease until the opposite intersection is reached at which point the strain would be zero again.

Analysis of the response of the gage due to skin friction was performed. The strain that is produced at each point in the silicon layer is related to depth, b, of the silicon layer at that point. The resulting relationship for the overall strain, e, is given by equation 4.2.

$$e=\frac{b\tau_w}{l_g G} \qquad [4.2]$$

Where τ_w is the skin friction which is taken for the model to be 500 Pa, G is the shear modulus for the silicon which is taken to be 7 x 10^6 Pa and l_g is the gage length (5.0 mm). Figure 4.7 is a graph showing how δ/l_g varies from the center of the groove out to the edge of the groove. Where δ is the change in length of the strain gage. A frequency response analysis was also performed to identify the sputtered gage's natural frequency. The predicted natural frequency of the sputtered gage is 185 kHz.

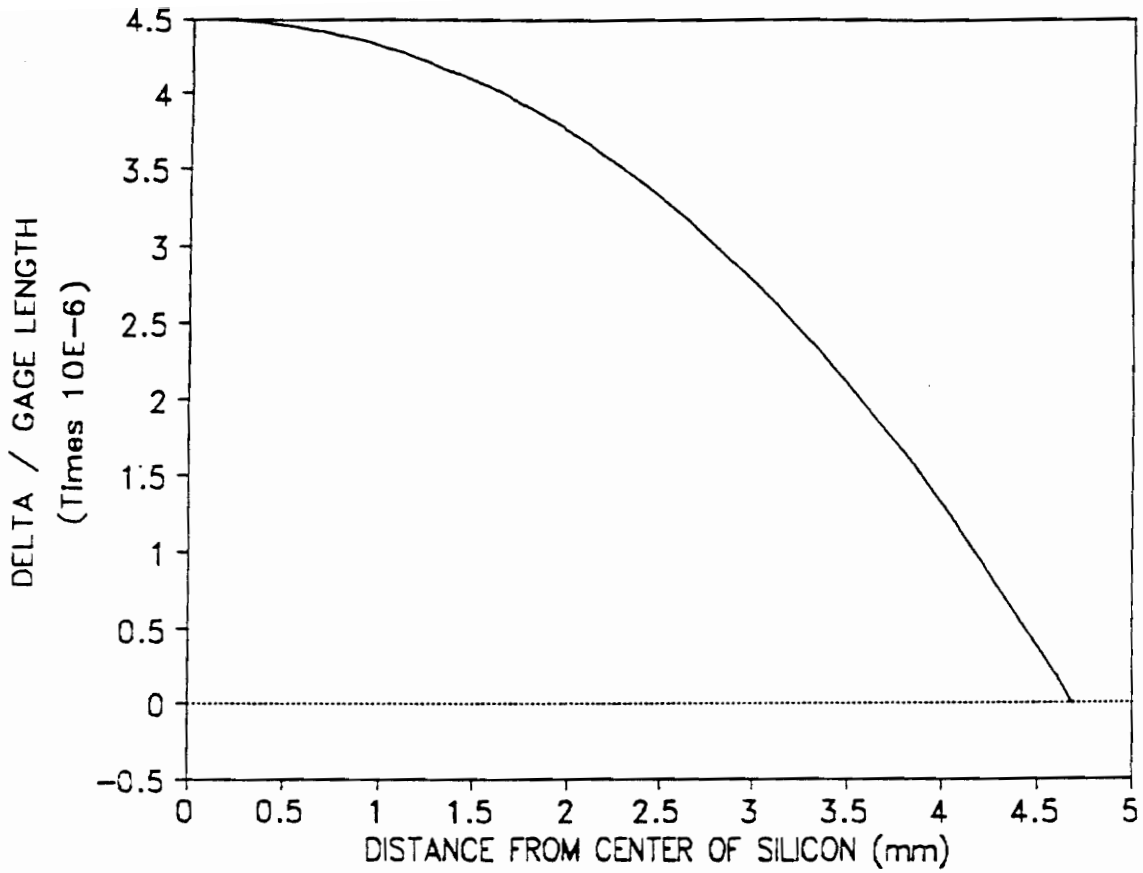

Figure 4.7 Graph of δ/l_g Versus Distance from Center of Silicon layer.

After the gage was analyzed and determined to be worthwhile to pursue, the sputtered skin friction gage was built for testing. Several problems were encountered with building the sputtered gage. One problem was getting the sputtered strain gages to hold a constant resistance. Dr. Onishi [21] a professor from the Bradley department of Electrical Engineering at Virginia Polytechnic Institute and State University, did the sputtering for the gage. He determined that the silicon rubber surface on which the sputtering done was rough and grainy. This surface roughness caused the thickness of the gage to vary across the surface of the silicon rubber. The varying thickness and rough surface caused the sputtered gage to experience microcracks. These microcracks affected the strain gage's resistance. Another problem was attaching the lead wires. Silver paint was first used, but the lead wires kept popping off. Feed through pin connections were used to eliminate the problem of lead wire attachments. This technology was borrowed from the Heat-Flux microsensor developed by Hager et al. [20]. With these pins the lead wire connections can be made behind the gage, leaving the surface of the gage smooth.

While the problem of lead wire attachments was solved, the problem of microcracks causing changes in overall strain gage resistance still needed a solution. For an ideal strain

gage it is desirable for the gage to change resistance only as a function of strain. Because these microcracks caused continuing change in strain gage resistance, reliable measurements were not possible.

Table 4.2 gives a list of the resistance of two sputtered strain gages along with the date the resistances were checked, and some notes about what was done with the gages prior to checking the resistances. Figure 4.8 graphically plots the change in resistance of these gages. The microcracks in the sputtered strain gages were a constant source of problems in the skin friction tests. Of all the sputtered strain gages that were made for testing, only one gave repeated tests without experiencing microcracks. Even this sputtered strain gage, changed resistance after several tests. This particular sputtered strain gage had a lower resistance than the others, because it was a little thicker. Attempts were made to reproduce other thicker sputtered strain gages that would not experience microcracks, but they were unsuccessful.

By using the sputtered gage that did last for several tests, some useful information was obtained. Oven tests, vacuum tests, and tunnel tests were performed to test the sputtered gage's temperature sensitivity, pressure sensitivity, and output due to high speed flow.

Table 4.2 Changes in Resistance of Sputtered Gages

NUMBER	DATE	EVENT	GAGE 1	GAGE 2
1	3/18/92	CHECK	710.8	700.9
2	3/19/92	CHECK	711.9	702.4
3	3/19/92	AFTER SOLDERING	712.0	702.7
4	3/19/92	AFTER FREE JET TESTS	747.7	1020.0
5	3/20/92	CHECK	749.1	813.0
6	3/23/92	CHECK	763.0	803.4
7	3/23/92	AFTER HEAT GUN TEST	755.5	765.5
8	3/23/92	AFTER HEAT GUN TEST	758.5	759.3
9	3/23/92	AFTER HEAT GUN TEST	757.3	780.7
10	3/23/92	BEFORE OVEN TEST	771.0	820.6
11	3/23/92	AFTER OVEN TEST	760.3	804.7

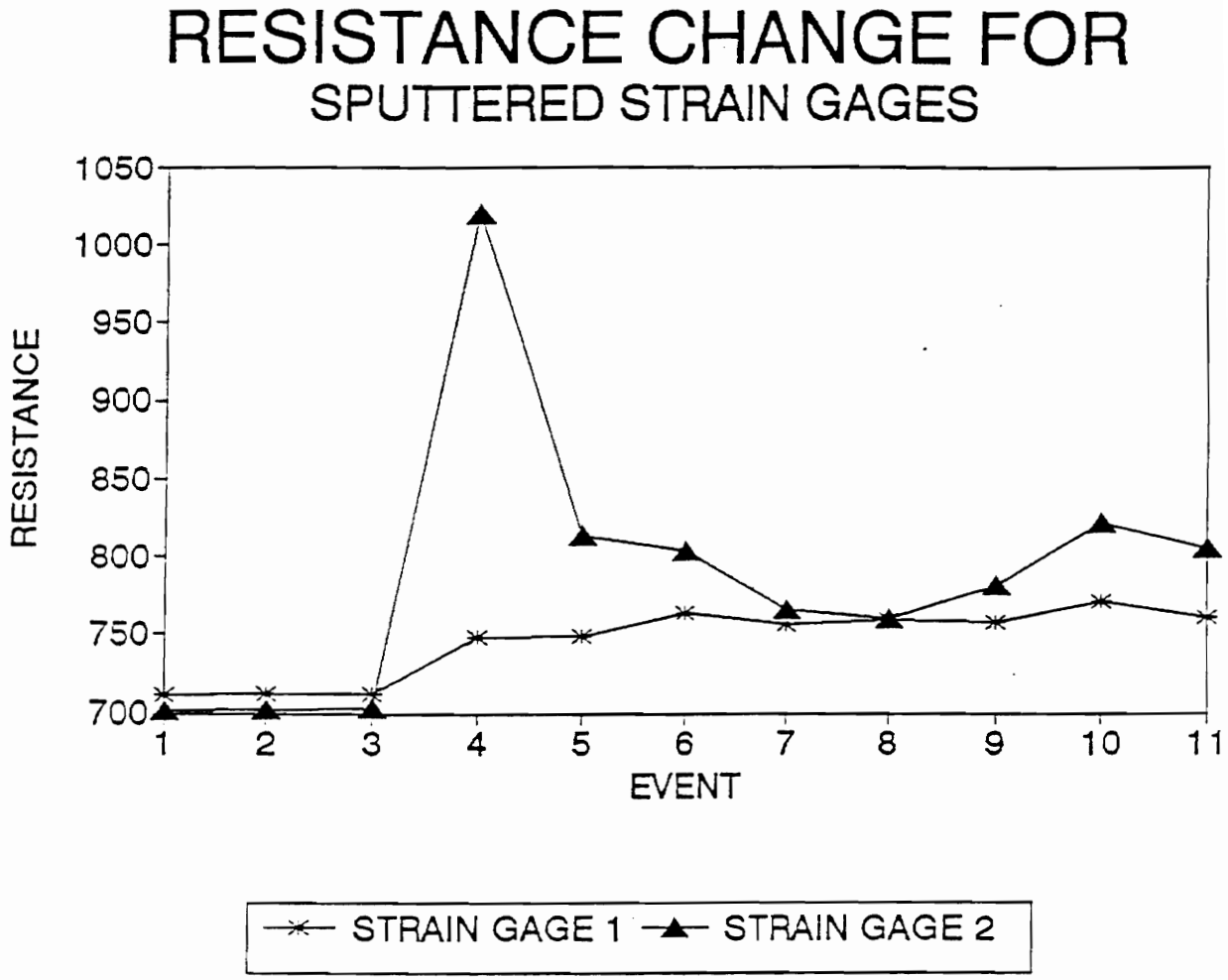

Figure 4.8 Graphical Representation of Resistance Changes

The oven tests were performed to quantify how the sputtered gage would react to changes in temperature. A sample of the output of one of the oven tests is given in figure 4.9. Channel one is the output from the sputtered gage. For this test the sputtered strain gage was wired into a Wheatstone quarter-bridge. With this configuration, the output from the bridge is directly related to the change of resistance of the sputtered strain gage. Channel two is the output from a type K thermocouple. For a total temperature rise of 5 degrees Celsius the change in output was 0.357 volts. Analysis of the system showed that the observed output was due to differential thermal expansion between the aluminum nitride plug and the silicon rubber, and not the thermal coefficient of resistance of the gage.

The vacuum tests were performed to determine how the gage output would be affected by the presence of a normal pressure. The gage was wired into a Wheatstone quarter-bridge configuration and then placed into a vacuum chamber. This chamber is attached by plastic tubing to a small vacuum pump. To run a test, the vacuum pump was turned on and the chamber was sucked down to an absolute pressure of 81 Pa. A sample of the output from these vacuum tests is provided in Figure 4.10. It is evident that the output due to normal pressure is small, (8 mV) compared to the output due to temperature. The output that does occur is probably due to the presence of air bubbles

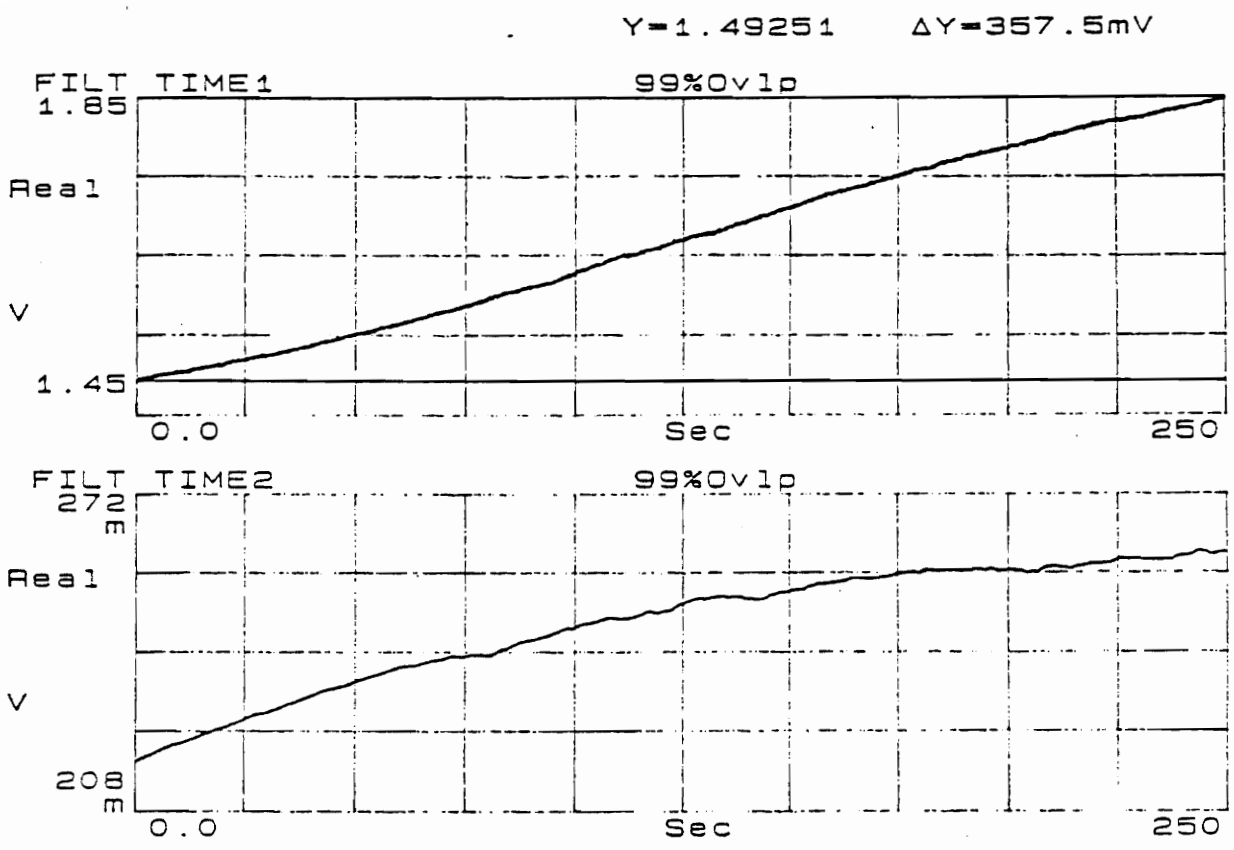

Figure 4.9 Oven Tests of the Sputtered Skin Friction Gage

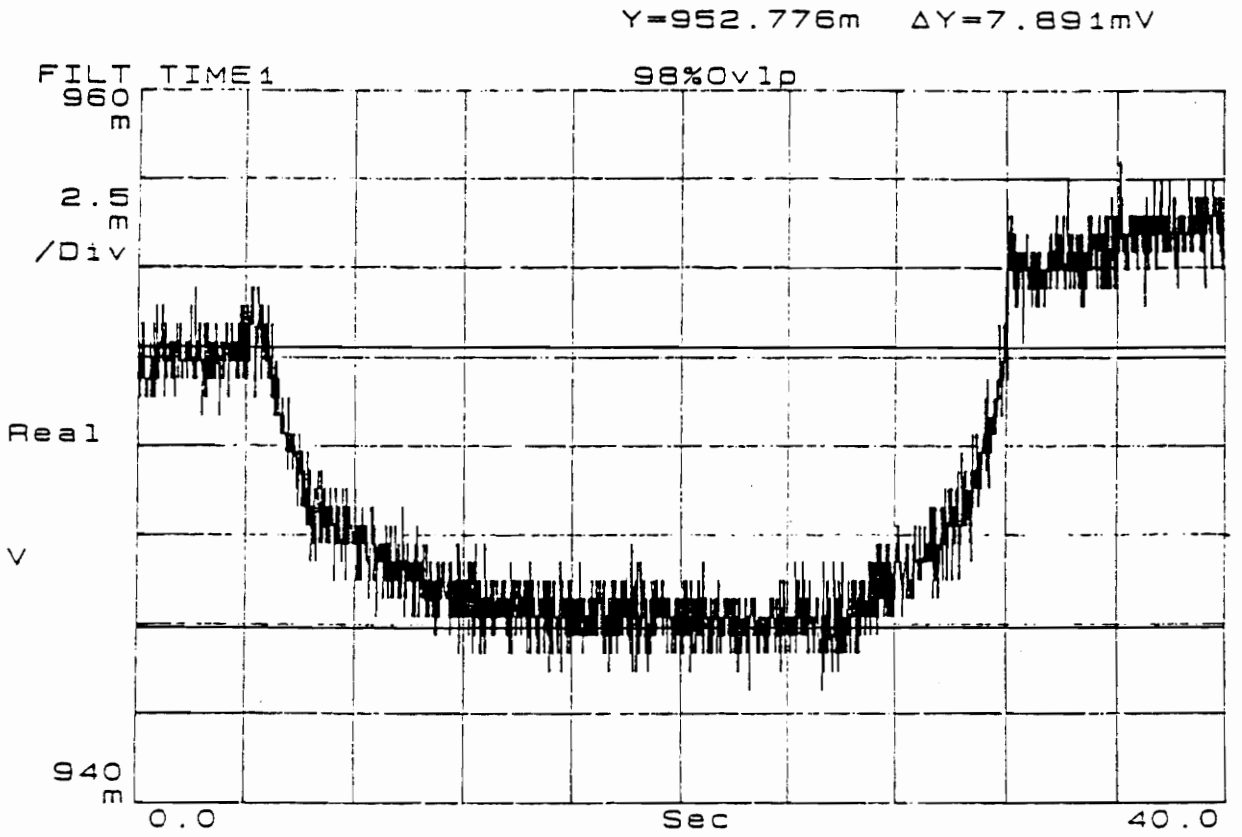

Figure 4.10 Vacuum Tests for the Sputtered Skin Friction Gage

in the silicon rubber. When air bubbles experience the vacuum pressure, they expand and produce strain in the sputtered strain gage. This problem can be reduced by applying the silicon rubber in the presence of a vacuum, thus eliminating most of the air bubbles.

A calibration of the sputtered gage was attempted using the viscometer. Several different angular velocities were tried, but the gage output drifted so much that it was impossible to record an accurate calibration.

4.6 FREE JET TESTS WITH SPUTTERED SKIN FRICTION GAGE

Several free jet tests were run with the sputtered skin friction gage in a Wheatstone quarter-bridge circuit. As expected from the oven tests, the output due to temperature was much greater than the output due to skin friction. Figure 4.11 shows the output from the Wheatstone quarter bridge circuit for the gage in all four testing positions. The zero position is with the strain gage in tension from the skin friction, while the one hundred eighty degree position produces compression in the sputtered strain gage. The 90 and 270 degree positions are perpendicular to the flow and thus shouldn't experience either tension or compression.

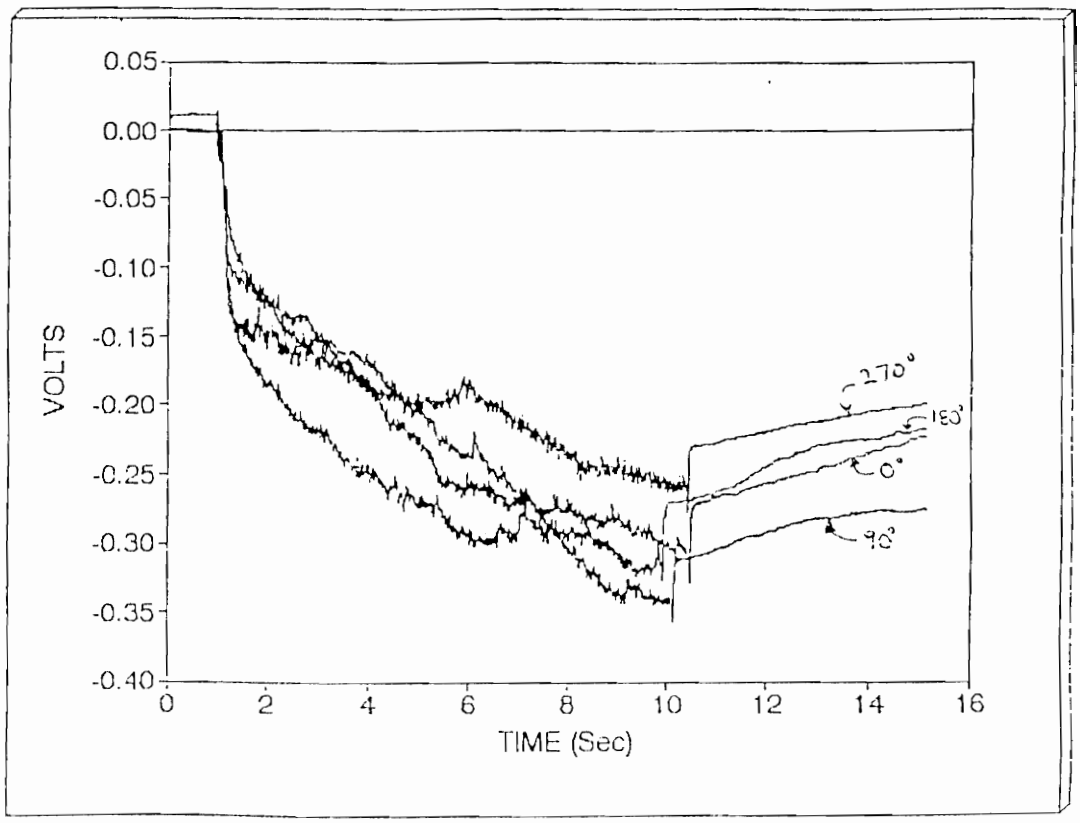

Figure 4.11 Free Jet Test Results for the Four Testing Positions

All four of the signals in figure 4.11 have the same shape and characteristics. This is because the temperature output is large compared to the skin friction output. In order to check the gage performance, compensation for the temperature effects was attempted by subtracting the signals. In using the Wheatstone half-bridge circuit, the temperature compensation is achieved automatically within the circuitry. Since a Wheatstone quarter-bridge circuit was used, temperature compensation can be achieved by subtracting one gage output from the other.

Figure 4.12 shows temperature compensation using the 180 and 0 degree outputs. The idea behind this temperature compensation is that the output due to temperature is the same for both tests while the output due to skin friction is the same magnitude but opposite in sign. When the output from 0 and 180 degrees are subtracted the temperature output should cancel while the output due to strain is doubled. Since 180 degrees corresponds to the strain gage in compression the output should be negative due to skin friction. When the positive output due to the tensile strain at zero degrees is subtracted from the 180 degree output, the result is a net negative output. This is what the result of figure 4.12 shows and the magnitude is close to what was predicted by the model (5.2 mV).

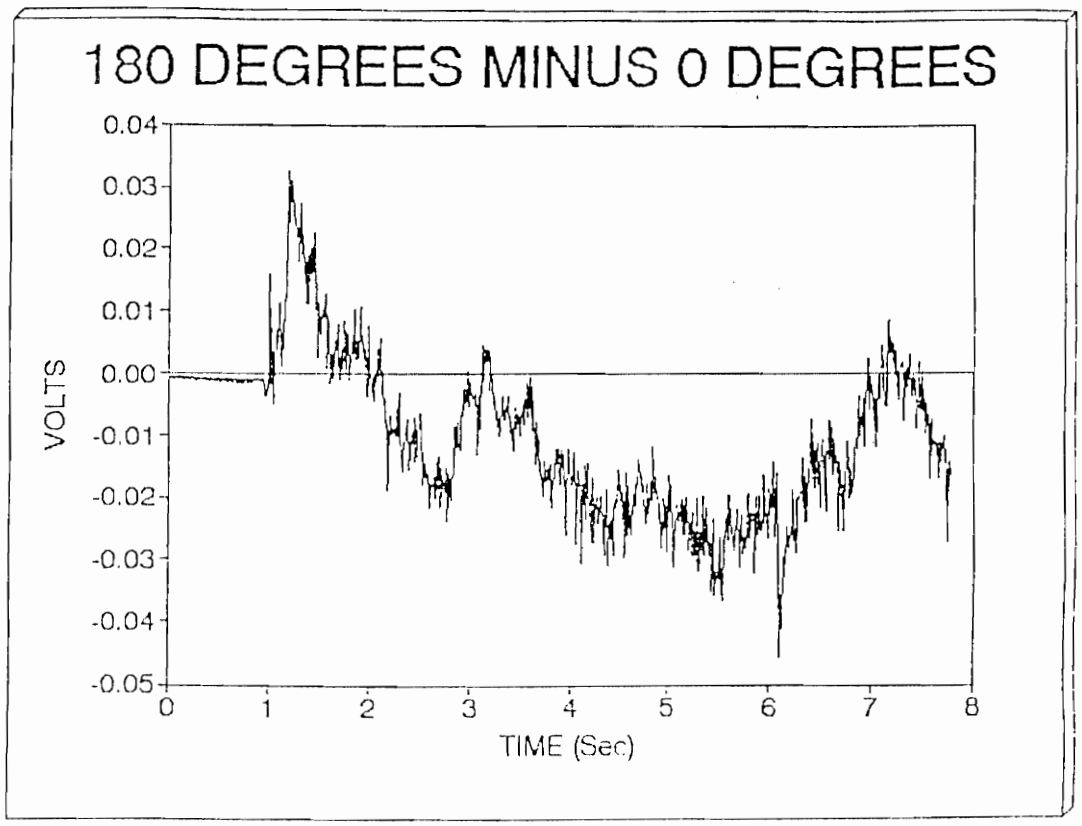

Figure 4.12 180 Degree Output Minus 0 Degree Output

The result from subtracting the outputs for the 0 and 180 degree positions seemed promising, so subtracting the outputs for 90 and 270 degrees positions was attempted next. Since both the 90 and 270 degree positions were perpendicular to the flow, the net output after compensating should be zero. Figure 4.13 shows the 270 degree output minus the 90 degree output. This output should be zero, but it is not. So while the results from the 0 and 180 degree temperature compensation seemed to be correct, the 90 and 270 degree compensation results contrary to the prediction.

The method of subtracting signals to accomplish temperature compensation was flawed because the gage outputs that were being subtracted came from different runs in the Free-Jet Facility. Further tests need to be made to determine if the sputtered skin friction gage is behaving as designed. Before further tests can be made; however, the problem of the sputtered gage microcracks needs to be solved. Once the sputtered strain gages can be made without the microcrack problem, the temperature compensation can be achieved automatically within the Wheatstone half-bridge configuration. Also quarter-bridge test can be run simultaneously and temperature compensation can then be made without worry of the error induced by compensating with different tests.

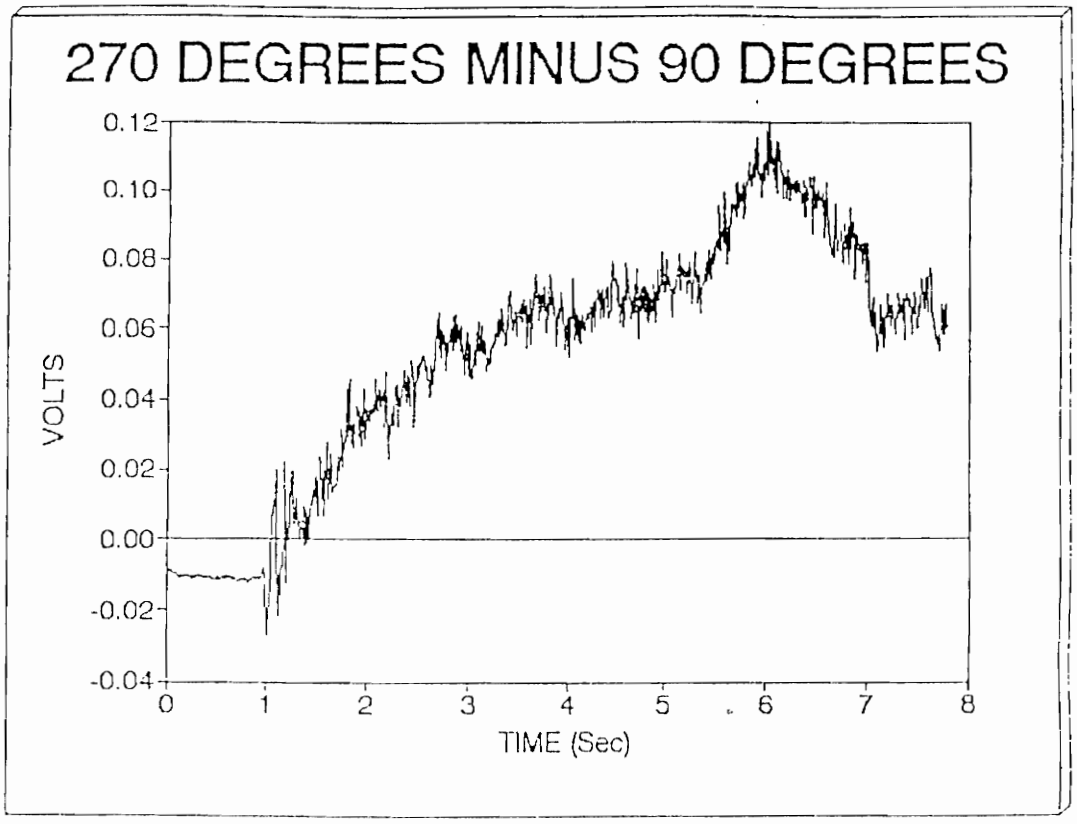

Figure 4.13 270 Degree Output Minus 90 Degree Output

4.7 T-TOP GAGE DESIGN

After determining that the temperature and pressure compensation techniques weren't adequate with the original gage design due to the distortion output, a new design was developed. This T-top gage was designed based upon the knowledge that was compiled with the previous gage designs.

Figure 4.14 is an assembly drawing of the T-top gage design. First, the T-top gage did not use the laser-cut thin film. It was the thin film that was the major reason for the output due to distortion. To reduce the temperature effects, the strain gages were placed one-eighth of an inch below the surface of the gage. The surface of this T-top gage is made of plexiglass so that the strain gages are insulated thermally. In order to reduce the pressure effects, two features were added. First, the sensing head was designed to float in a five mil thick layer of silicon rubber. This silicon rubber, plus the geometry of the sensing head, help to keep the sensing head from flexing up or down due to normal pressures. The second feature to reduce pressure effects is the threaded rod that fastens the sensing head in place. The plexiglass base plate and backing are mounted to a steel body by screws, and the strain gage lead wires are fed out of the back.

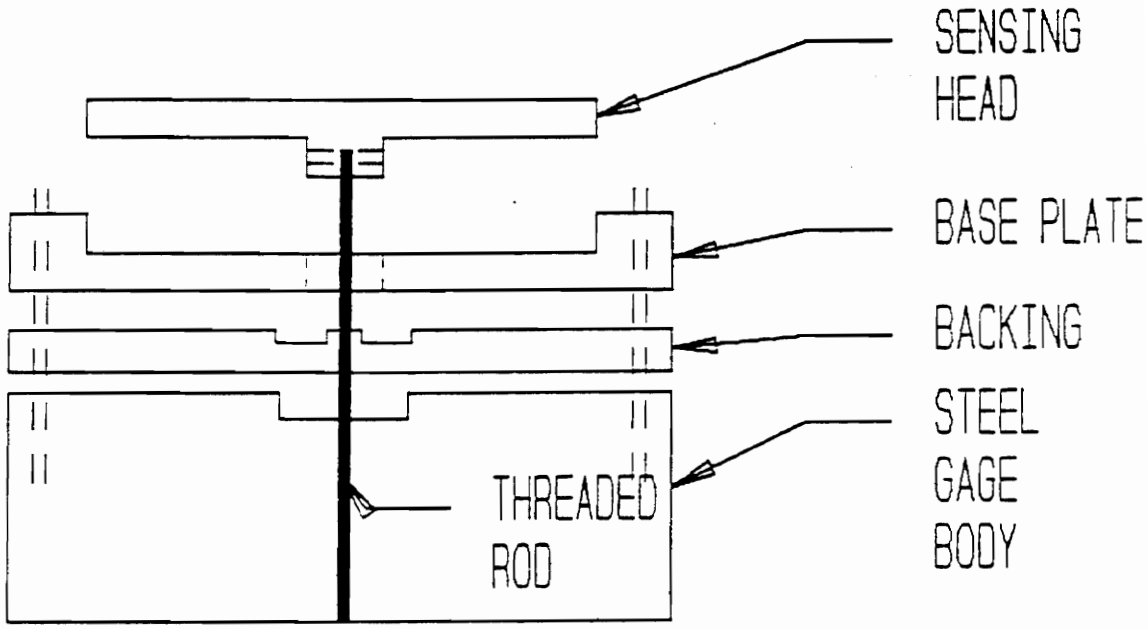

Figure 4.14 Assembly drawing of T-top gage design

4.8 RESULTS OF T-TOP GAGE TESTS

Since the design for this T-top gage is different than any of the previous designs, the first priority was to determine the T-top gage's physical characteristics. This included analyzing the frequency response and physically modeling the T-top gage. The steady gage output due to skin friction was predicted for the Free-Jet Facility. A natural frequency for the gage of 12 kilohertz was also predicted.

In order to experimentally determine the frequency response of the T-top gage, a shaker and a ZONIC spectrum analyzer were used. The T-top gage was mounted on the shaker along with a force transducer. White noise was input by the shaker over a wide frequency band. A power spectrum plot of the T-top gage, and a coherence plot between the gage output and the force transducer were taken with 200 averages. Figures 4.15 and 4.16 are the power spectrum and coherent plots for the 0 and 180 degree axis, while Figures 4.17 and 4.18 are the power spectrum and coherence plots for the 90 and 270 degree axis. The power spectrum plots for both axes show that the natural frequency for the T-top gage is approximately 11 kilohertz. This is close to the 12 kilohertz natural frequency that was predicted by the model. There is also high

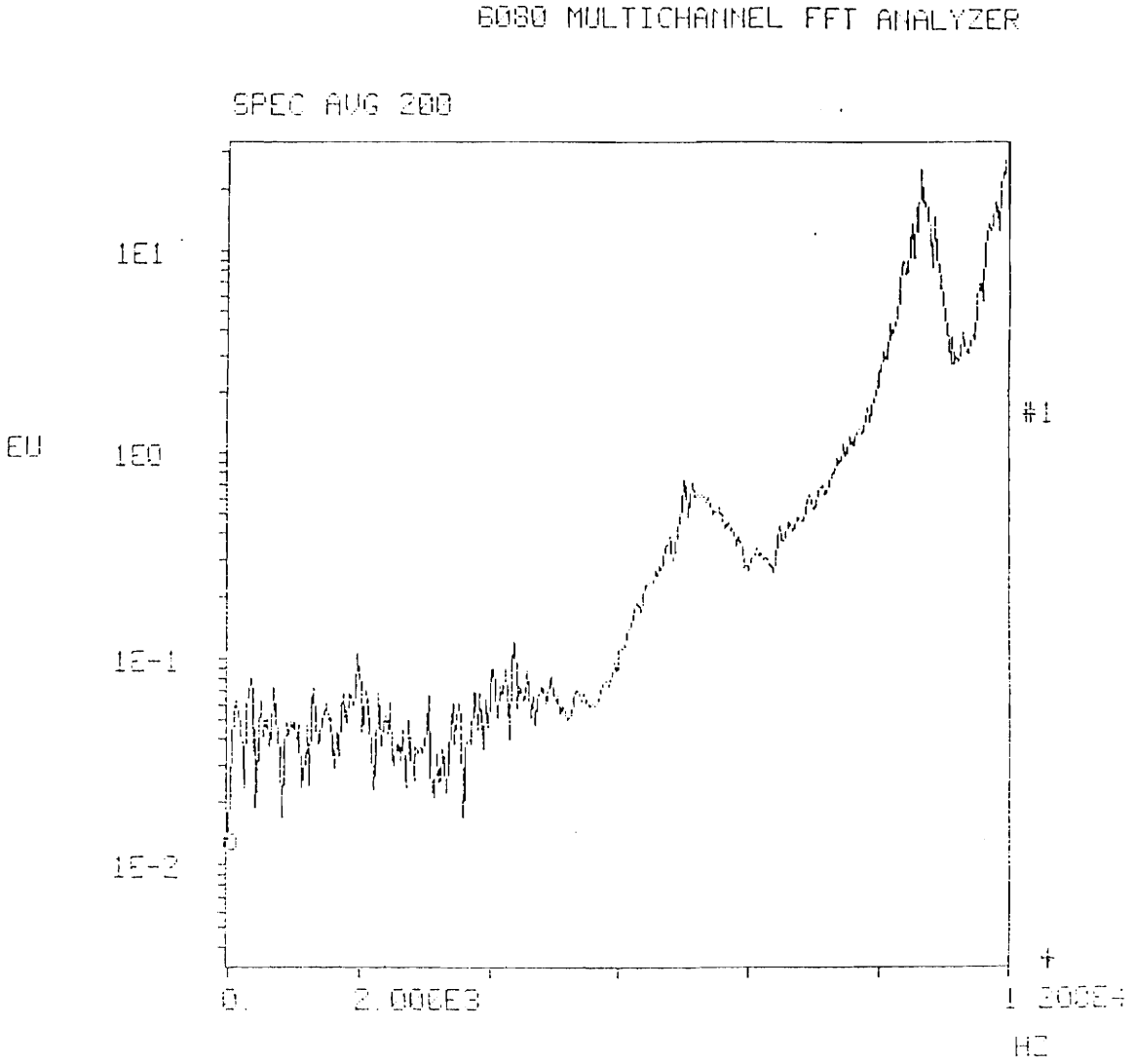

Figure 4.15 Power Spectrum for 0 and 180 Degree Axis

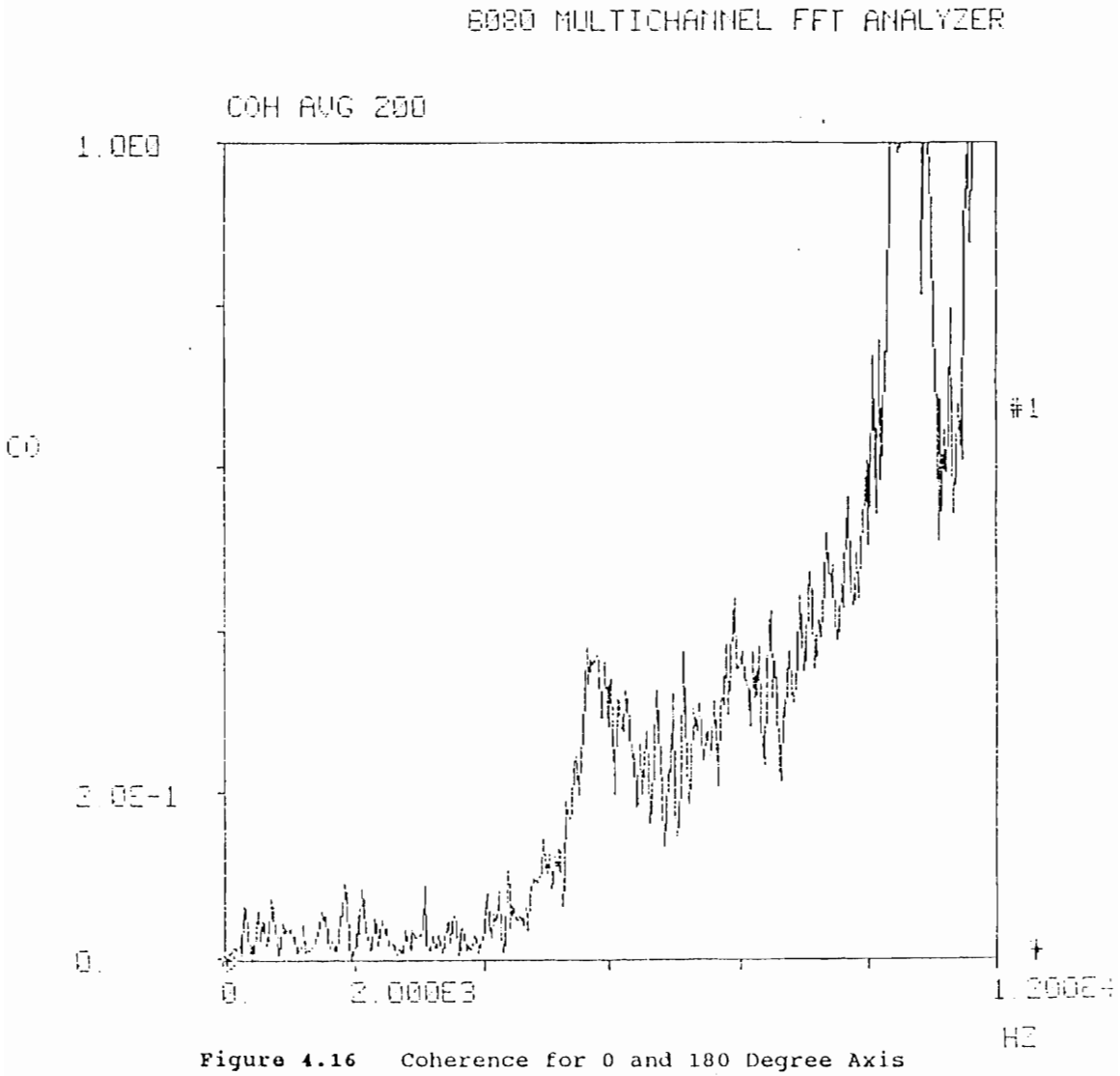

Figure 4.16 Coherence for 0 and 180 Degree Axis

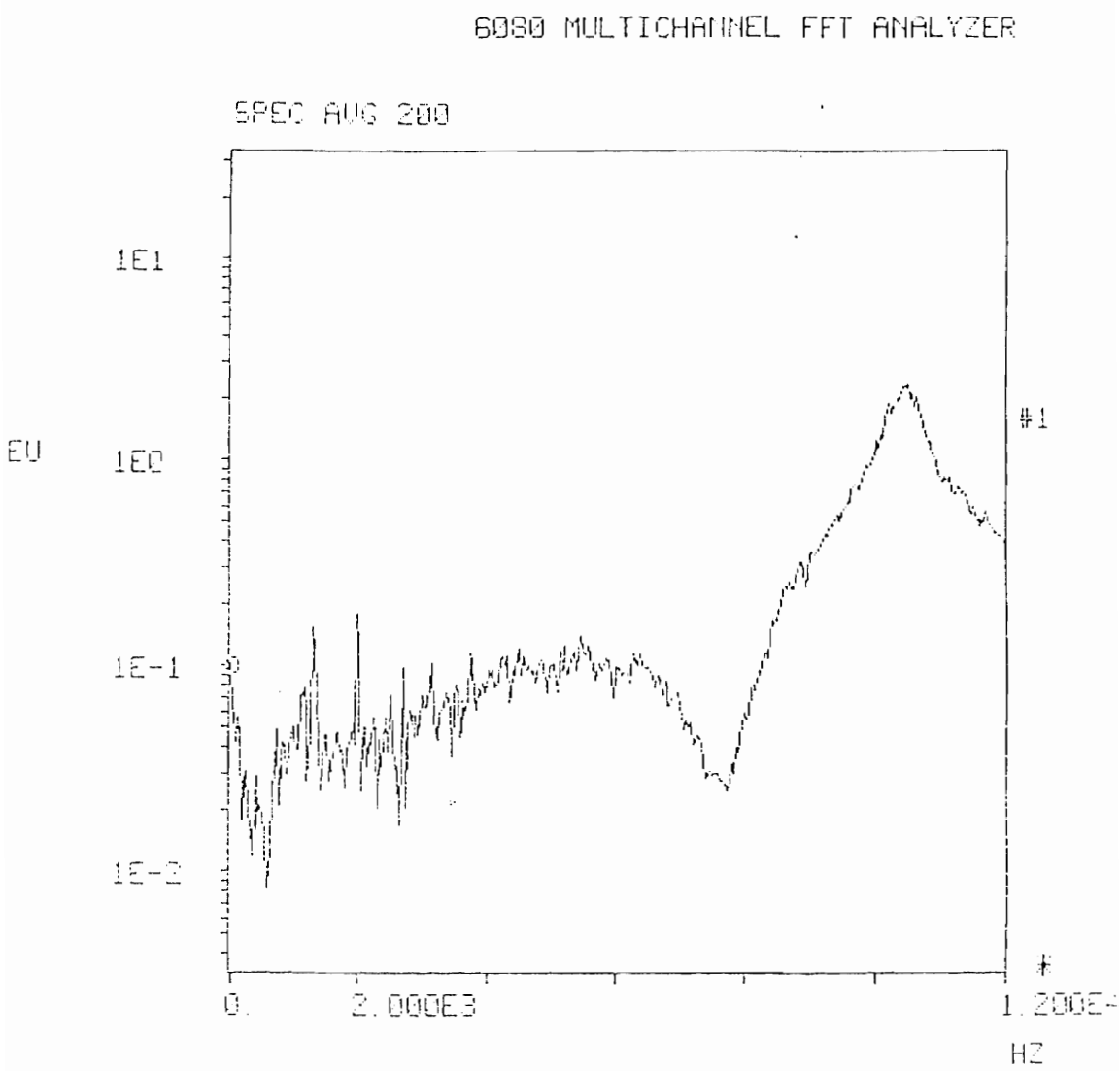

Figure 4.17 Power Spectrum for 90 and 270 Degree Axis

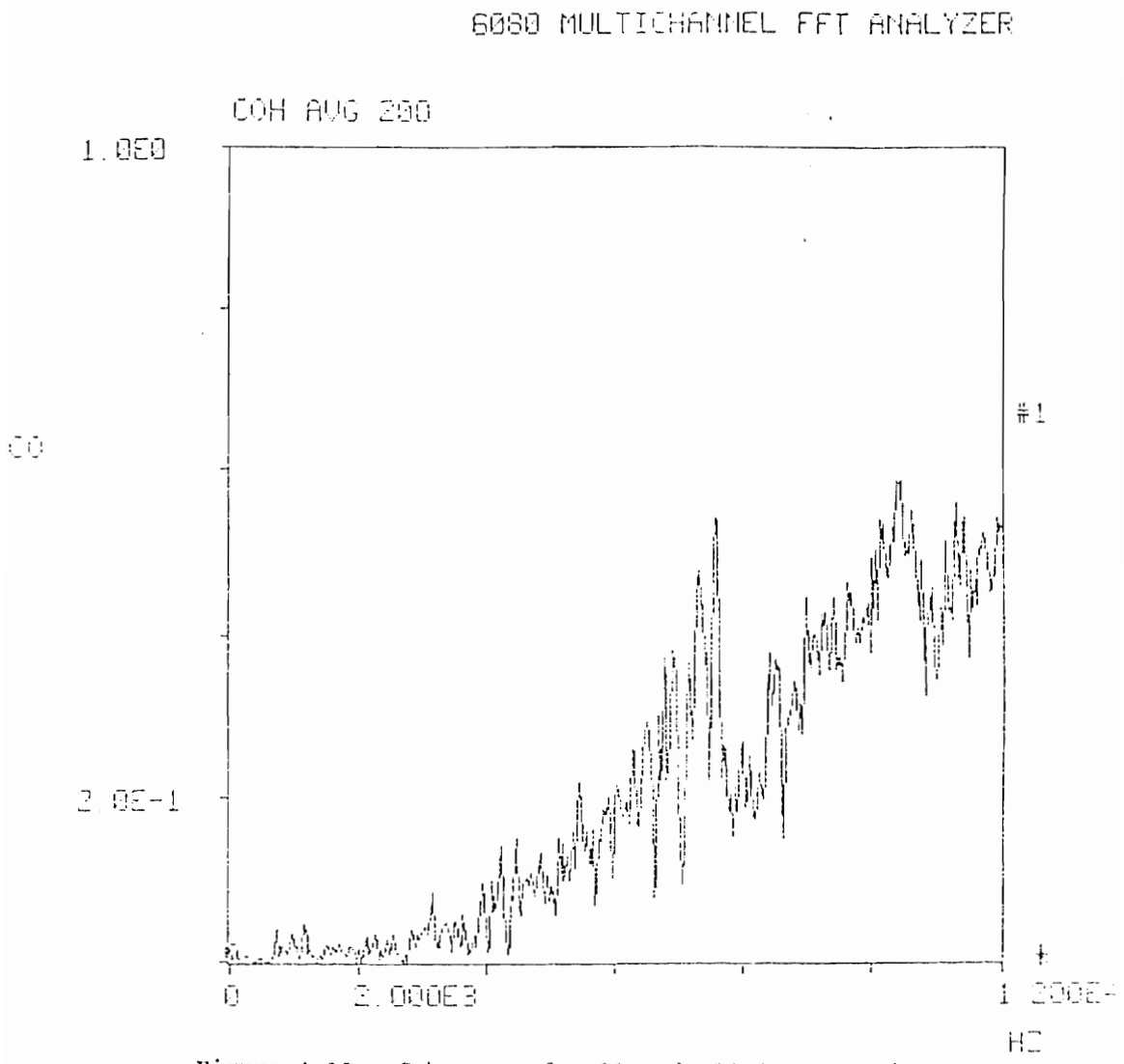

Figure 4.18 Coherence for 90 and 270 Degree Axis

correlation between the force transducer and the gage output around the natural frequency of 11 kilohertz. From the power spectrum plots it can be shown that measurements can be made accurately in the frequency range up to five kilohertz.

A static calibration was performed for this T-top gage design. This calibration was done by hanging weights from a thread that was attached to the sensing head. A graph of the calibration is provided in figure 4.19.

Free-jet tests were run with the T-top gage design to determine how the gage would perform in high speed flow. A sample of the output for one of the tests is provided in Figure 4.20. This figure shows the output for the 0 and 180 degree strain gages, both hooked up in a Wheatstone quarter bridge configuration. Quarter bridges were chosen so that the effect of the air flow on each individual strain gage's change in resistance could be determined. The new skin friction gage was positioned so that the 0 degree strain gage would be in compression and the 180 degree strain gage would be in tension. From the T-top gage calibration and strain gage theory, the 0 degree output should be negative and the 180 degree output should be positive.

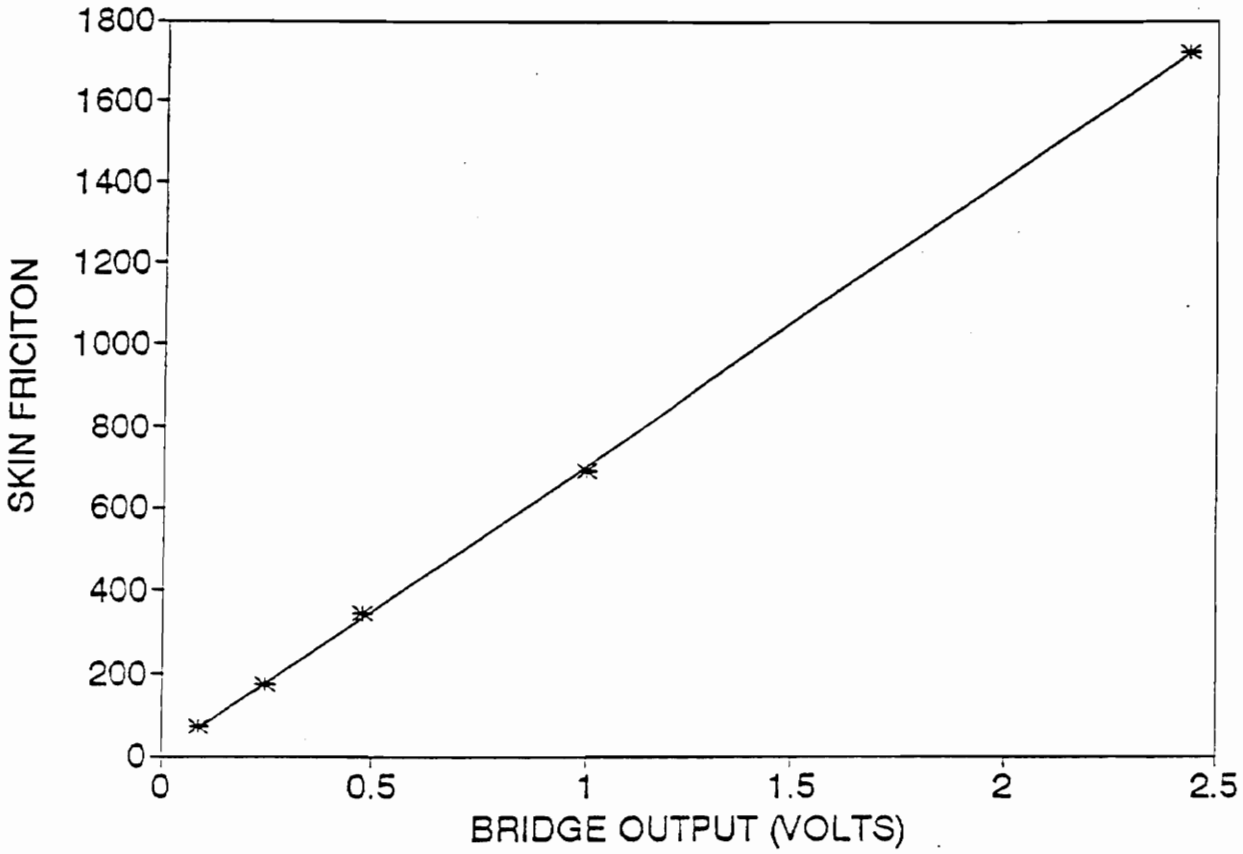

Figure 4.19 Calibration for T-top gage

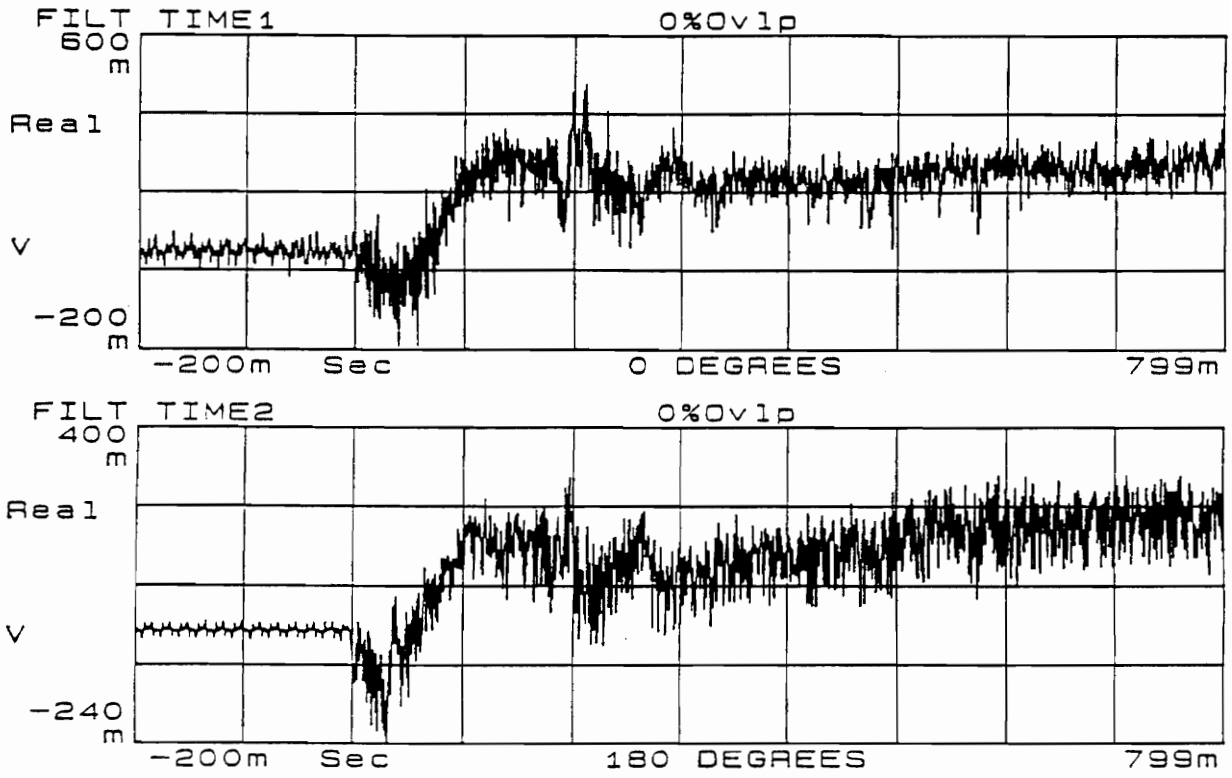

Figure 4.20 Output for Free Jet Tests with the T-top Gage

While the output of the strain gages are approximately the correct magnitude as determined from the calibration, the direction for the signal of the 0 degree output is not correct. The 0 degree output should be negative because the strain gage is in compression. One possible reason for this measurement error is a small rocking motion that can occur with this sensing head configuration. If small rocking motions do occur, stresses could be produced in the strain gages that would be unrelated to the skin friction.

Chapter 5

CONCLUSIONS AND RECOMMENDATIONS

5.1 CONCLUSIONS

Although skin friction was never successfully measured with the present gage designs, many of the problems associated with skin friction measurement were pinpointed. These problems were determined to be as follows:

- The isolation of the much smaller skin friction signal from the larger normal pressure.
- The output due to temperature effects
- The making of a sputtered strain gage that will hold a constant resistance.

Several methods were developed and tested for eliminating the first two problems. The sputtered skin friction gage showed some promise, but further testing cannot be made until a way of making sputtered strain gages that hold a constant resistance is developed.

The T-top gage design was determined to have a natural frequency of 11 kHz. This T-top gage had a really nice linear calibration, but didn't perform as expected in supersonic flow. The error of the T-top gage in supersonic flow was suspected to be caused by rocking motion of the sensing head.

5.2 RECOMMENDATIONS

The following recommendations are given for future work with the sputtered skin friction gage.

- Determine a method for sputtering the strain gages so that they hold a constant resistance.
- Perform a calibration in the viscometer to determine the response of the sputtered gage to various levels of skin friction.
- Make tests with the sputtered skin friction gage in the shock tube developed by Yagnavulkya Mukkamala.

The following recommendations are given for future work with the T-top gage design.

- Use ball bearing or roller bearings under the sensing head instead of silicon rubber so that the sensing head will not be able to rock at all.
- Make tests with the T-top gage design in the shock tube developed by Yagnavulkya Mukkamala.

REFERENCES

1. Deturris, D. J., Schetz, J.A., and Hellbaum, R.F., "Direct Measurements of Skin Friction in a Scramjet combustion," AIAA paper No. 90-2342, 1990.

2. Hanratty, T.J. & Campbell, J.A ., 1983. "Measurement of Wall Shear Stress" in Fluid Mechanical Measurements (ed. R.J. Goldstein). Hemisphere Publication Corporation, pp. 559-615

3. East, L.F., "Measurement of Skin Friction at Low Subsonic Speeds by the Razor-Blade Technique", Aero. Res. Counc. London, R & M 3525, 1966

4. Preston, J.H., "The Determination of Turbulent Skin Friction by Means of Pitot Tubes", J. R. Aero. Soc., Vol. 58, pp. 109-121, 1953.

5. Patel, V.C., "Calibration of the Preston Tube and Limitations on Its Use in Pressure Gradients", Journal of Fluid Mechanics, Vol. 23, Part I, 1965, pp. 185-208.

6. McAllister, J.E., Pierce, F.J., & Tennant, M.H. 1982 "Preston Tube Calibrations and Direct Force Floating Element measurements in a Two-Dimensional Turbulent Boundary Layer" Journal of Fluids Engineering, pp. 156-160

7. Head, M.R. & Rechenberg, I., "The Preston Tube as a Means of Measuring Skin Friction", Journal at Fluid Mechanics, Vol. 14, pp. 1-17, 1962.

8. Fage, A. and Falkner, V.M. "On the Relation Between Heat Transfer and Surface Friction and Laminar Flow," Aero. Res. Counc., Lond, R & M No. 1408.,1931

9. Bellhouse, B.J., & Schultz, D.L. "Determination of Mean and Dynamic Skin Friction, Separation, and Transition in Low-Speed Flow with a Thin-Film Heated Element," Journal of Fluid Mechanics, Vol. 24, pp. 379-400, 1966.

10. Bellhouse, B.J., & Schultz, D.L. "The Measurement of Fluctuating Skin Friction in Air with Heated Thin-Film Gauges," Journal of Fluid Mechanics, Vol. 32, part 4, pp. 675-680, 1968.

11. Diller, T.E., Onishi, S., Langley, L.W. Hager, J. M., Simmons, S., & Smith, D. "Experimental Performance of a Heat Flux Microsensor," June, 1990.

12. Mitchell, J.E. & Hanratty, T.J., "A Study of Turbulence at a Wall Using an Electrochemical Wall-Stress Meter", Journal of Fluid Mechanics, Vol. 26, pp. 199-221, 1966.

13. Winter, K.G., "An Outline of the Techniques Available for the Measurement of Skin Friction," Prog. Aerosp. Sci., vol. 18, pp. 1-57, 1977.

14. Putz, James M., Master of Science Thesis - "Development of a Direct Force Reading Thin Film Shear Stress Gage," Virginia Polytechnic Institute and State University, January, 1991.

15. Putz, John M., Master of Science Thesis - "The Development of Instrumentation for the Support of Skin Friction and Heat Flux Measurements," Virginia Polytechnic Institute and State University, March, 1991.

16. Perry, C. C., and Lissner, R. H., "The Strain Gage Primer," McGraw-Hill Book Company, Inc., New York, 1955.

17. Bowersox, R., Personal Communication, April 1992.

18. Mills, John R., Master of Science Thesis - "A Mach 1.95 Free-Jet Facility For Experimental Investigation of Injectant Flow Patterns," Virginia Polytechnic Institute and State University, October 1991.

19. Mukkamala Yagnavulkya., Personal Communication, May 1992.

20. Hager, J. M., Simmons, S., Smith, D., Onishi, S., Langley, L. W., and Diller, T. E., "Experimental Performance of a Heat Flux Microsensor," ASME Paper No. 90 GT, 1990.

21. Onishi, S., Personal Communication, April 1992.

APPENDIX A

DEVELOPMENT OF SKIN

FRICTION INSTRUMENTATION

SUBMITTED BY

JOHN BUSIC

ON

APRIL 22, 1991

TABLE OF CONTENTS

PROBLEM STATEMENT

The purpose of this Independent Study research is to determine the feasibility of using the new heat flux gage developed by Dr. T.E. Diller and S. Onishi to measure skin friction. Initial testing was done to analyze the performance of the gage in a steady, low speed wind tunnel. A Preston tube was used to calibrate the gage to skin friction measurements. This paper details the initial experiment and its results.

BACKGROUND THEORY

The basic thrust of this research is to take the heat flux gage and to calibrate it for skin friction measurements. This is done by using a Preston tube and the heat flux gage. The Preston tube is a small measuring device that works much like a Pitot tube. The Preston tube differs in that it is usually much smaller (0.028 inches in diameter) and it is placed right at the surface of the plate. The Preston tube measures the difference between the dynamic pressure and the static pressure at the surface of the plate. The Patel Preston tube calibrations[1] were then used to convert the measured difference in pressure to the wall shear stress or skin friction.

The heat flux gage that was used is a gage that was originally developed and patented by Dr. T.E. Diller and S. Onishi, and made by Vatell[2]. This gage has been shown to have a very high frequency response and that it can measure very high heat flux. The gage consists of approximately one hundred thermocouple pairs in series. The thermocouple pairs determine temperature difference across a known thermal resistance. With this information, the heat flux can be determined. The gage gives an output voltage that is directly proportional to the heat flux.

Heat flux is directly related in many cases to the local surface skin friction. There is a formula that relates skin friction to heat flux[3]. The formula is:

$$\frac{q''}{\Delta T}=A+B(\rho\tau)_w^{1/3}$$

q'' is the heat flux as determined by the gage. ΔT is the temperature difference between the surface of the gage and the room temperature. The Greek letter Roe (ρ) is the density of the air stream and the Greek letter Tau (τ) is the skin friction and the lowercase w means that these values are evaluated at the plate surface. A and B are calibration constants that depend mildly on ΔT and can be obtained from the y-intercept of the plots of q'' divided by ΔT versus the skin friction and the log-log of q'' divided by ΔT versus the skin friction.

In order to get an idea of what values to expect before experimentation began, certain pressure differences for the Preston tube were calculated for a range of tunnel velocities. To accomplish this, standard atmospheric conditions were used for air. Since the plate length was determined by the experimental set up and a range of velocities were to be used, a range of Reynolds numbers could be calculated. From each Reynolds number the corresponding local coefficient of

friction could be determined, and once the local coefficient of friction was known, the local surface skin friction could be determined. Once all of these values were determined, the expected pressure difference for the Preston tube was determined using the Patel Preston tube calibration equations. A FORTRAN program was written to calculate the expected pressure difference for the Preston tube for a range of velocities.

EXPERIMENTAL PROCEDURE

In order to calibrate the heat flux gage for skin friction measurements, the heat flux (q''), the difference in temperature between the gage surface and the room temperature (ΔT), and the skin friction at the gage surface (τ_w) had to be measured. Once these values were determined, they could be plotted and the equation constants A and B could be determined.

The heat flux and the difference in temperature between the gage surface and the room temperature could be measured with the heat flux gage. The skin friction at the surface of the gage was measured with a Preston tube.

In order to take the necessary data, a low speed wind tunnel was used. At the end of this tunnel was placed a sheet of plyboard with the Preston tube and the gage placed flush with the surface and 24.5 inches from the leading edge. The heat flux gage was hooked up to the amplifier and the signal was measured with a Hewlett Packard Signal Analyzer. This signal analyzer provided signals that were directly related to the heat flux and the surface temperature of the gage. The Preston tube was hooked up to a manometer that measured the difference between the dynamic pressure and the static pressure at the surface of the plyboard.

In order to get several different data points, the velocity of the tunnel had to be varied. This was accomplished by either decreasing the exit area of the tunnel (higher velocity) or restricting the intake of the fan (lower velocity). A typical experiment was carried out as follows. The Hewlett Packard Signal Analyzer was directed to start taking data from the gage. Next the tunnel was turned on and allowed to reach steady flow conditions. After the signal analyzer acquired the necessary data it was paused. Then the Preston tube manometer was read, and then the tunnel was shut down. This provided the heat flux data, the surface temperature of the gage, and the skin friction for a certain tunnel velocity. This was done six different times in order to get enough data to plot the curves. The data from each of the six runs is given in the Table 1.

TABLE 1: EXPERIMENTAL DATA

TEST NUMBER	T_w (Pa)	q''	ΔT
1	1.45	12,296	54.3
2	1.49	11,827	54.3
3	2.24	12,851	54.0
4	1.23	10,943	54.0
5	0.69	8,528	55.4
6	1.54	10,011	51.8

EXPERIMENTAL RESULTS

The experimental results were very promising. At 27 meters per second, the predicted pressure difference was about 147 Pascal, and the Preston tube gave a pressure difference of 139.5 Pascal. This showed that the turbulent boundary layer was well behaved and close to standard conditions. Once the Preston tube was determined to be giving accurate results, the heat flux gage could be calibrated using the Preston tube results. To get the local skin friction at the gage surface, the pressure difference measured with the Preston tube was converted to skin friction by using the Patel Preston tube calibration equations.

Six different runs were made with the tunnel and data was taken for each of the six runs. The heat flux is given as an output voltage (7.36mV is equivalent to one watt per centimeter squared). A sample graph of the heat flux and the temperature of the gage surface as output voltages is provided in figure 1. The output voltage given is negative. This means that the heat is being given off by the gage into the air. In order to determine the actual heat flux, the average heat flux once the tunnel reaches steady state is determined and then subtracted by the initial heat flux at time equal to zero (the heat flux that was present before the tunnel was turned on). The slow initial drop is due to the starting time

of the wind tunnel. Determining the corresponding surface temperature of the gage is a little more involved. As the heat is being given off at the surface of the gage, the temperature at the surface of the gage is changing. In order to get one value for the surface temperature, the average temperature of the gage surface once the tunnel reaches steady state is used. The gage gives an output voltage that is directly proportional to the surface temperature. Once the local skin friction, the surface temperature of the gage, and the heat flux are known, the heat flux divided by the difference in temperature can be plotted against the skin friction. A sample calculation of the skin friction, the temperature difference, and the heat flux for one set of data is given in the Appendix. The plots of q'' divided by ΔT versus skin friction and the log-log of q'' divided by ΔT versus skin friction are given in figures 2 and 3 respectively. From these plots the constants A and B were determined to be 5.2 and 170 respectively.

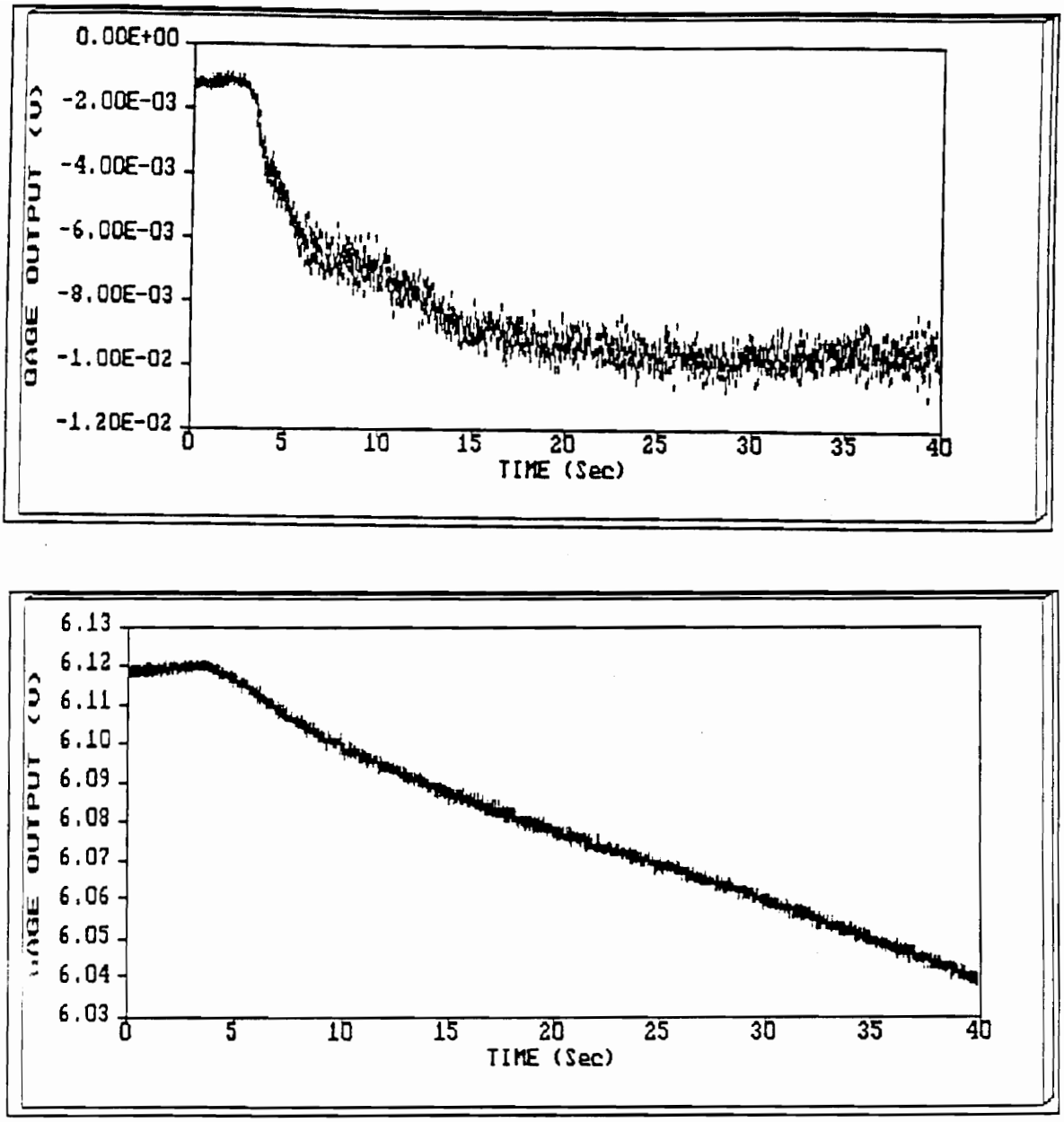

Figure 1 Gage Output versus Time (Heat Flux and Temperature)

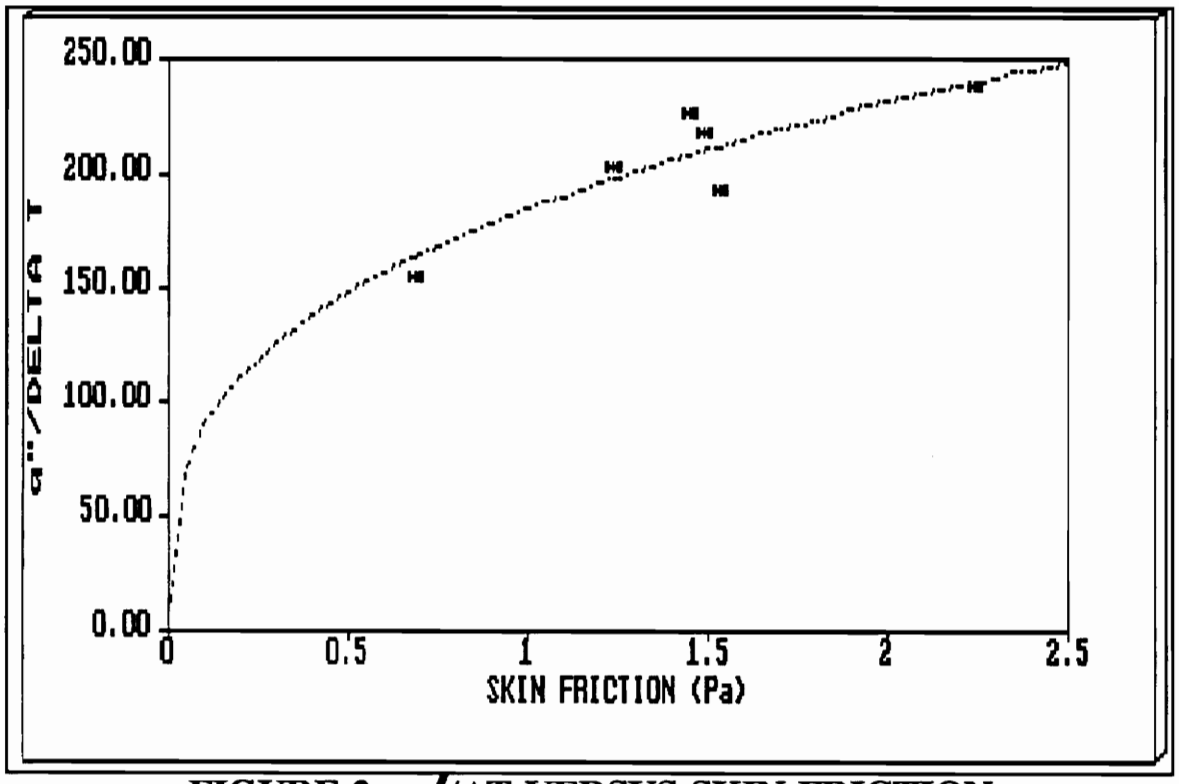

FIGURE 2: $q''/\Delta T$ VERSUS SKIN FRICTION

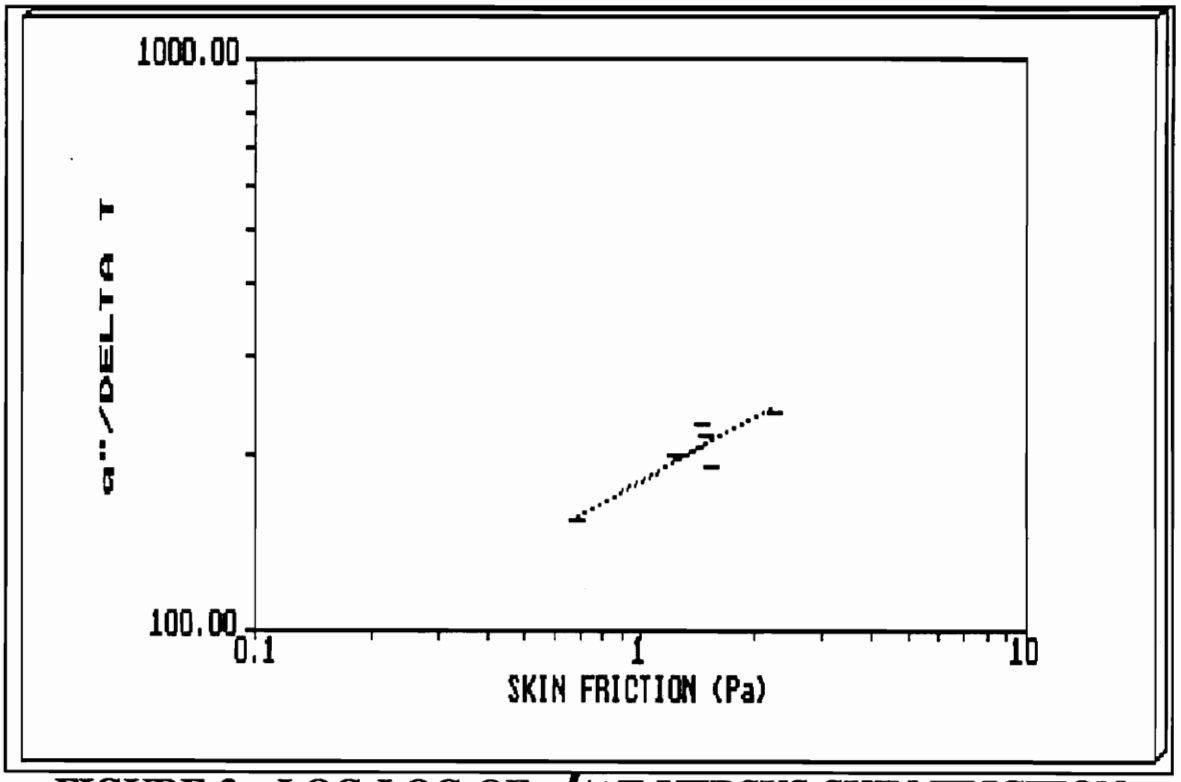

FIGURE 3: LOG-LOG OF $q''/\Delta T$ VERSUS SKIN FRICTION

RECOMMENDATIONS

The data and the plots of the data that were achieved through this experiment were close to what was predicted through theory. The log-log plot was supposed to have a slope of one-third, and it was determined by a linear reqression of the log-log data to be about 0.36. This was close enough to what was predicted to assure that this research should continue and that it is possible to calibrate the heat flux gage for skin friction measurements, at least in steady flow situations. The next step in this research project would be to test the gage again to see if this data can be repeated. It would be beneficial to achieve a more accurate calibration of the gage. Eventually the gage should be tested in unsteady and supersonic flow. For an initial test of this gage as a skin friction measuring device, this experiment went very well.

REFERENCES

[1]Patel, V.C., "Calibration of the Preston Tube and Limitations on Its Use in Pressure Gradients," Journal of Fluid Mechanics, Vol. 23, Part 1, 1965, pp. 185-208

[2]Diller, T.E., and Onishi, S., VPI & SU, Hager, J.M., and Langley, L.W., Vatell Corporation, Christiansburg, VA. "High Temperature Heat Flux Measurements," 29th Aerospace Sciences Meeting Jan. 7-10, 1991/Reno Nevada. AIAA 91-0165

[3]Diller, T.E., and Telionis, D.P., "Time-Resolved Heat Transfer and Skin Friction Measurements in Unsteady Flow," in Advances in Fluid Mechanics Measurements, Lecture Notes in Engineering, Ed. M. Gad-el-Hak, Springer-Verlag, Berlin, 1989, pp. 323-355.

APPENDIX

SAMPLE CALCULATIONS FOR DETERMINING:

SKIN FRICTION

ΔP FROM THE PRESTON TUBE = 139.5 Pa.

USE THE PATEL PRESTON TUBE CALIBRATION TO GET

$\underline{T_w = 1.45 \text{ Pa}}$

TEMPERATURE DIFFERENCE

THE AVERAGE OUTPUT VOLTAGE ONCE THE TUNNEL REACHED STEADY STATE WAS 6.06 V.

THE CALIBRATION EQUATION FOR CONVERTING VOLTS TO DEGREES CELSIUS IS: $-354 + 71 \times \text{VOLTS} = \text{TEMPERATURE}\ (°C)$

USING THIS CALIBRATION THE TEMPERATURE = 79.3 °C

THEREFORE ΔT = 79.3 °C - 25 °C = $\underline{54.3\ °C}$

HEAT FLUX

THE GAGE OUTPUT VOLTAGE DIFFERENCE = 9.05 mV.

HEAT FLUX ,IN WATTS PER SQUARE CENTIMETER, IS DETERMINED BY DIVIDING THE VOLTAGE (IN MILLIVOLTS) BY 7.36.

$q'' = 9.05/7.36 = 1.2296\ W/cm^2 = \underline{12{,}296\ W/m^2}$

APPENDIX B

Calculation of expected skin friction from the free jet facility

Known: $P_0 = 689$ kPa $M = 2.0$

$T_0 = 298$ oK $\gamma = 1.4$

$R = 0.287$ kJ/(kg oK)

$$\frac{P_0}{P} = \left(1 + \frac{\gamma - 1}{2} M^2\right)^{\frac{\gamma}{\gamma - 1}} \qquad (1)$$

Solve equation (1) for P: $P = 88{,}116$ Pa

$$q = \frac{P \gamma M^2}{2} \qquad (2)$$

Now solve for q using equation (2): $q = 246{,}724$ Pa

$$C_f = \frac{\tau_w}{q} \qquad (3)$$

Using equation (3) and assuming $C_f \cong 0.002$, Solve for τ_w:

$$\tau_w \cong 493.4 \text{ Pa}$$

VITA

John Franklin Busic was born in St. Louis, Missouri on February 7, 1968. He moved when he was two years old and considers Gloucester County, Virginia to be his home town. After graduating from Gloucester High School in 1986, he began his undergraduate studies at Carson-Newman College in Jefferson City, Tennessee. It was at Carson-Newman where he met his future wife. He transferred to Virginia Tech to complete his undergraduate studies in the fall of 1989. He received his Bachelor of Science in Mechanical Engineering on May 4, 1991 and was married to Meredith Marie Booth on May 5, 1991. The writing of this thesis concludes a Master of Science in Mechanical Engineering program started in May of 1991. Upon conclusion of his Masters Degree John Busic will start work at the Naval Surface Warfare Center in Dahlgren, Virginia.

John F. Busic